https://doi.org/10.5194/egusphere-2024-4075
Preprint. Discussion started: 22 January 2025

Dynamic vegetation reveals unavoidable climate feedbacks and their dependence on climate mean state

Pascale Braconnot*, Nicolas Viovy and Olivier Marti

Laboratoire des Sciences du climat et de l'environnement (LSCE-IPSL, unité mixte CEA-CNRS, UVSQ, Université Paris Saclay, Orme des Merisiers, 91191 Gif sur Yvette Cedex, France
*corresponding author : pascale.braconnot@lsce.ipsl.fr

Abstract. We investigate seasonal vegetation feedbacks considering mid-Holocene and pre-industrial simulations with the IPSL climate models for which dynamic vegetation is switch on. We consider four different settings for the land surface model designed to improve the representation of boreal forest. They combine different choices for bare soil evaporation, photosynthesis and associated parameters, and tree mortality. Whatever the model set up, the major seasonal differences expected between the mid Holocene and preindustrial climates remain similar, and consistent with the mid Holocene greening of the Sahara and northward shift of the northern limit of forest in the northern hemisphere. However, the way vegetation-climate interactions trigger unavoidable radiative surface albedo and water vapor feedbacks depend on the model content. Cascading feedbacks involve local snow-vegetation interactions, as well as remote water vapor and long wave radiative feedbacks in the tropics, which are needed to fulfill the global energy conservation constraint of the climate system. We show that the parameterization of bare soil evaporation is a key factor that control tree growth in mid and high latitudes. Photosynthesis parameterization appears to be critical in controlling the functioning of vegetation and vegetation-climate interactions. It affects the seasonal evolution of the vegetation and leaf area index, as well as their effect on radiative feedbacks and the sensitivity of the vegetation feedback to the climate mean state. This sensitivity needs to be considered when developing and tuning climate models.

1 Introduction

Green Sahara and the northern limit of forest in the northern hemisphere are key characteristics of the differences between the mid Holocene and present-day climate (i.e. Jolly et al., 1998; Prentice et al., 1996). Vegetation change during the mid-Holocene has been in the Paleoclimate Modeling Intercomparison Project (PMIP) since the beginning (Joussaume and Taylor, 1995), either to understand vegetation changes and feedback on climate (i.e. Claussen and Gayler, 1997; Texier et al., 1997) or for model evaluations purposes (i.e. Harrison et al., 1998, 2014). Interactive coupling, either asynchronously or synchronously, have highlighted some of the key feedbacks induced by vegetation changes and the way vegetation affect land albedo, soil properties or teleconnections (Joussaume et al., 1999; Levis et al., 2004; Pausata et al., 2017). These past studies have emphasized the role of the snow albedo feedback in mid and high latitudes. Typical examples concern the role of vegetation-snow albedo feedback in last glacial inception (Gallimore and Kutzbach, 1996; de Noblet et al., 1996). Fully coupled Earth System models with asynchronous coupling or online dynamical vegetation also highlight the role of indirect feedbacks of the vegetation with ocean circulation or sea-ice, amplifying the initial vegetation effect or providing a muted response in these mid and high latitudes (Gallimore et al., 2005; Otto et al., 2009b; Wohlfahrt et al., 2004). It also raises

https://doi.org/10.5194/egusphere-2024-4075
Preprint. Discussion started: 22 January 2025

concerns on the strength of forest-snow albedo feedbacks affecting the temperature signal in spring (Otto et al., 2011).

These earlier questions are still there. In the last 10 years the increase number of transient Holocene simulations has emphasize complementary questions on the fact that vegetation could be an important factor to consider to reconcile the simulated temperature evolution in the early Holocene with climate reconstruction (Dallmeyer et al., 2022; Liu et al., 2014; Marsicek et al., 2018; Thompson et al., 2022). They also raised questions on the relationship between long term changes in vegetation, external forcing and variability (Braconnot et al., 2019), as well as on boreal forest tipping points (Dallmeyer et al., 2021). However only a limited number of studies considers the fully coupled climate-vegetation dynamic system in these investigations. Despite the fact that models are becoming more complex and that there is a growing number of models with fully interactive carbon cycle, there is still a small number of modeling groups using model configurations with fully interactive vegetation (see Arias et al., 2021). Transient Holocene simulations with dynamical vegetation show broad agreement on the mid-Holocene green Sahara and boreal forest, but there are still lots of discrepancies in many regional aspects of the responses and large model biases in the representation of vegetation as the one discussed by Braconnot et al. (2019). These difficulties come both from differences in the vegetation and land surface model (Hopcroft et al., 2017), and from the fact that first order climate-vegetation interactions in a fully interactive system are not well understood.

Climate-vegetation feedbacks are somehow hidden in the land surface albedo and atmospheric moisture feedback in estimates of climate sensitivity (Sherwood et al., 2020). They have a direct effect on temperature, controlling vegetation, leaf area index, productivity, evapotranspiration, soil moisture, as well as snow and ice cover. They cannot be easily quantified because they depend on the mean climate state and, when it comes to simulations, to the simulated climate mean state characteristics (Braconnot and Kageyama, 2015). A reason is that vegetation lies at the critical zone between land and atmosphere. Its variations depend on interconnected factors such as light, energy, water and carbon and, in turn, affect climate and environmental factors. These interconnexions makes it difficult to disentangle the exact factors that affect the representation of vegetation in a fully interactive model. Dynamical vegetation introduces additional degrees of freedom in climate simulations, so that a model that produces reasonable results when vegetation is prescribed might not be able to properly reproduce the full coupled system, when climate-vegetation interactions that are neglected when vegetation is prescribed induce first order cascading effects in coupled mode. Vegetation feedbacks are in general overlooked when developing climate models or comparing simulations performed with different models. There is thus a risk that the linkages between the model content is not properly accounted for in model comparisons, since part of the results might come from vegetation-climate feedbacks that can themselves be tight to the underlying mean climate state.

Here we investigate the climate-vegetation feedback in mid-Holocene and pre-industrial simulations with the IPSL climate models using four different settings of the dynamical vegetation that combining differences in the choice of the representation of photosynthesis, bare soil evaporation and parameters defining the vegetation competition and distribution. The objective is to investigate the first order cascading climate-vegetation feedbacks, and to identify their dependence to the model content and the climate mean state. We first compare the mid-Holocene climate changes obtained with the different model versions. The mid-Holocene climate is a key reference period for

https://doi.org/10.5194/egusphere-2024-4075
Preprint. Discussion started: 22 January 2025

paleoclimate modeling, characterized by enhanced seasonality in the northern hemisphere and reduced seasonality in the southern hemisphere compared to present day (Kageyama et al., 2018; Otto-Bliesner et al., 2017). It is well suited to investigate feedbacks occurring at the seasonal time scales, such as those induced by the seasonal evolution of vegetation in response to the seasonal cycle of the insolation forcing in mid and high northern latitudes. A focus is put on the estimations of the atmospheric feedbacks resulting from surface albedo, atmospheric water content and lapse rate following Braconnot and Kageyama (2015). We analyse the dependency of these first order feedbacks to the representation of vegetation, and relate this to the model content, and how it affects the vegetation-climate interactions. The aim is to highlight key factors controlling the unavoidable feedbacks induced by snow and ice cover or by atmospheric water content through evaporation and temperature in a fully coupled system. We also focus on the differences in these feedbacks between the model versions considering the mid-Holocene and the preindustrial climates separately, so as to understand the dependence of the seasonal feedbacks on the climate mean state.

The reminder of the manuscript is organized as follow: Section 2 presents the set-up of the four model configurations and the suite of experiments. Section 3 is dedicated to the analyses of the differences between the mid-Holocene and the preindustrial climates, including a quantification of the atmospheric feedbacks resulting from the response to the mid-Holocene insolation forcing. Section 4 goes deeper in the analyses of the feedbacks considering the differences between the mid-Holocene simulations and making the linkages between these differences and the model content, before addressing the questions of the feedback dependence to the climate mean-state. The discussion and conclusion, section 5, highlights the key findings and the implications for the land carbon sources and sinks.

2 Model and experiments

2.1 IPSL model and different settings of the land surface component ORCHIDEE

The reference IPSL Earth climate model version for this study is IPSLCM6-LR (Boucher et al., 2020). This model version has been used to produce the suite of CMIP6 simulations experiments (Eyring et al., 2016), including the mid Holocene PMIP4-CMIP6 (Braconnot et al., 2021). The atmospheric component LMDZ (Hourdin et al., 2020) has a regular horizontal grid with 144 points regularly spaced in longitude and 142 in latitude (2.5° × 1.3°) and 79 vertical layers extending up to 80 km. The land surface component ORCHIDEE version v2.0 is run using the atmospheric resolution. It includes 11 vertical hydrology layers and 15 plant functional types (Cheruy et al., 2020). The ocean component NEMO (Madec, Gurvan et al., 2017) uses the eORCA 1° nominal resolution and 75 vertical levels. The sea ice dynamics and thermodynamics NEMO-LIM3 (Rousset et al., 2015; Vancoppenolle et al., 2009) and the ocean biogeochemistry NEMO-PICES (Aumont et al., 2015) are run at the ocean resolution. The oceanic and atmospheric components are coupled through the OASIS3-MCT coupler (Craig et al., 2017) with a time step of 90 mn.

Compared to the PMIP4-CMIP6 mid Holocene simulations (Braconnot et al., 2021), the dynamical vegetation module (Krinner et al., 2005) is switch on for all the simulations considered in this study. The vegetation dynamics is based on the approach of the LPJ model (Sitch et al., 2003). It allows to simulate the evolution of the vegetation

https://doi.org/10.5194/egusphere-2024-4075
Preprint. Discussion started: 22 January 2025

cover in response to climate. It accounts for several climate constraints (e.g. minimum and maximum temperature) for vegetation fitness and competition between plant functional types (PFTs) based on their relative productivity Starting from this reference version, two formulations of bare soil evaporation and photosynthesis have been tested. These tests have been motivated by an underestimation of the boreal forest when using the standard version of the dynamical module in IPCLCM6-LR (see below). The test made on bare soil evaporation uses developments described in details in the documentation of ORCHIDEE hydrology by Ducharne et al. (2018). In the standard version of the IPSLCM6-LR, model bare soil evaporation depends on the moisture content of the first 4 of the 11 soil layers (Milly, 1992). The bare soil evaporation rate corresponds to the potential evaporation rate when the moisture supply meets the demand (Cheruy et al., 2020). Another solution has been developed to better represent soil evaporation processes, by considering the ratio (*mc*) between the moisture in the litter zone (first four surface layers) and the corresponding moisture at saturation (Sellers et al., 1992). With this parameterization, the aerodynamic resistance is decreased by a factor $\frac{1}{rsoil}$, where:

$$rsoil = e^{8.206-4.255*mc} \tag{1}$$

This adjustment in the bare soil evaporation parameterization was not incorporated into IPSLCM6A-LR due to the fact that it induces a surface warming that was not fully understood to be used in the whole suite of CMIP6 simulations (Cheruy et al., 2020). For simplicity, the two parameterizations are respectively referred to as *bareold* and *barenew* in the following (Table 1).

TABLE 1

The parameterization of photosynthesis/stomatal conductance used in the ORCHIDEE land surface model (Fig. 1) is different between IPSLCM5A-LR (Dufresne et al., 2013) and IPSLCM6-LR (Boucher et al., 2020). In IPSLCM5A-LR (Fig 1), the photosynthesis (PhotoCM5) is represented by the standard Farquhar model for C3 (Farquhar et al., 1980) which has been extended to C4 plants (Collatz et al., 1992) and coupled to the Ball & Berry stomatal conductance formulation (Ball et al., 1987). In IPSLCM6-LR (Fig. 1), the photosynthesis/conductance (PhotoCM6) has been improved to include the approach based on Yin and Struik (2009) coupled to the original Farqhuar (1980) model. The PhotoCM6 parameterization allows to replace the iterative resolution by an explicit solving of the coupled photosynthesis/stomatal conductance. Important differences between the two approaches are due to the fact that the stomatal conductance is driven by the vapor pressure deficit in PhotoCM6, whereas in PhotoCM5 it is based on relative humidity. Also, the shape of the response of the photosynthesis to temperature is different (Fig. 1). The temperature response is a bell shape function in PhotoCM5, which allows to control the minimum, maximum and optimal temperature of photosynthesis independently of the maximum rate of photosynthesis. The response of photosynthesis to temperature is driven by a modified Arrhenius function in PhotoCM6, with a reference temperature of 25°C. Hence the fixed maximum rate of carboxylation *Vcmax* it the rate at 25°C, whereas it is the optimal *Vcmax* in PhotoCM5 (Fig. 1), and the parameters (named ASJ) of the Arrhenius function are prescribed. It does not allow to have a full control on the temperature response, which is the reason why we reimplemented the PhotoCM5 parameterization to run our tests with IPSLCM6-LR. Another important difference is that in PhotoCM6, the response to temperature is adapted to the local long term (i.e. 10 years) temperature of each pixel whereas in PhotoCM6, the temperature dependence is fixed for the whole *pft*.

https://doi.org/10.5194/egusphere-2024-4075
Preprint. Discussion started: 22 January 2025

FIG1.

These differences in the shape of the function has some implication on some of the adjustments we made to the original parameterizations to compensate for the tendency of the climate model to be too cold in some mid to high latitude regions (Boucher et al., 2020). The objective was to allow photosynthesis at lower temperature. The parameters of photoCM6 have been adjusted using off line simulations forced by atmosphere reanalysis. The objective was to find optimal limits in temperature for PhotoCM6 and to adjust *Vcmax* at 25°C and ASJ within acceptable range of values. In the standard version of the IPSLCM6-LR model these parameters are the standard ones, and we add an *s* to the name in that case (Table 1). The photoCM5 parameterization use the standard values of PhotoCM6.

Another important process determining the possibility for forest to grow in a cold environment is the critical temperature for tree regeneration (*tcrit*). Indeed, it is assumed that, even for boreal forest, a very low temperature during winter will induce an insufficient fitness for reproduction and then forest regeneration. In the standard model version, it is prescribed to -45 °C for boreal evergreen needle leaf forest (pft 7) and boreal deciduous broadleaf forest (pft 8). It means that when daily temperature goes below 45°C a fraction of trees dies. This threshold was too high as currently regions covered with forest regularly experience temperatures under -45 °C. We therefore changed the critical temperature to -60 °C, the standard value used for Larix (pft 9), taking the risk to simulate a wrong composition of boreal forest.

2.2 Experiments

We consider a set of four experiments (Table 1). For each of them, we performed a mid-Holocene simulation following the PMIP4-CMIP6 protocol (Otto-Bliesner et al., 2017) as in Braconnot et al. (2021), and a pre-industrial CMIP6 simulations (Eyring et al., 2016). The preindustrial climate we use as reference in this study has a similar Earth’s orbit configuration as today, with summer solstice occurring at the perihelion and winter solstice at the aphelion. These experiments represent key steps in a wider range of tests designed to improve the representation of boreal forest. Model developments were done using the mid-Holocene as a reference for natural vegetation, knowing that the preindustrial climate is affected by land use, which is not considered in these experiments.

The different model set ups for these simulations are gathered in Table 1. The first experiment, V1, is performed with the standard model and the dynamical vegetation switch on. The differences with the simulations presented in Braconnot et al. (2021) are thus only due to the dynamical vegetation climate interactions. All the other experiments include the new parameterization of bare soil. Experiment V2 and V3 have the PhotoCM5 parameterization of photosynthesis. In V3 the critical temperature is modified for boreal forests. The final version V4 is parallel to V3, using PhotoCM6 photosynthesis. Note also that some bugs and inconsistent choices when running with or without the dynamical vegetation have been found in the standard model version after the first experiment was completed. They have been corrected for the sensitivity tests and do not affect the results that only focus on key factors that have emerged from a large suite of shorter systematic sensitivity experiments. Note that version V4 is considered as the reference version for ongoing Holocene transient simulation with dynamical vegetation.

https://doi.org/10.5194/egusphere-2024-4075
Preprint. Discussion started: 22 January 2025

The initial state for all the simulations corresponds to a restart of the IPSLCM6-LR model for the ocean-atmosphere-sea-ice-icesheet system. The land-surface model starts from bare soil. We follow here the protocol used by Braconnot et al. (2019). It guaranties the entire consistency between the simulated climate and the simulated vegetation. We tested that, as in our previous set of Holocene experiments with dynamical vegetation (see Braconnot et al., 2019), the results would be the same when a vegetation map from a previous simulation is used as initial state. This is mainly due to the fact that the land surface covers only ~30 % of the Earth and doesn't store energy on a long-time scale, compared to the ocean. The initial state corresponds to a mid-Holocene or PI climate depending of the simulated period, except for the preindustrial simulation using V4 for which the initial state is from the mid-Holocene simulation (Table 1).

2.3 Vegetation-climate adjustments

A similar sequence is found for the vegetation adjustment time in all experiments (Fig. 2). Starting from bare soil imposes a land surface cold start, since bare soil has a larger albedo than grasses or forest. It is characterized by a negative heat budget at the surface (Fig. 2b), a colder 2m air temperature (Fig. 2c), reduced precipitation and atmospheric water content (Fig. 2d, e), increase sea ice volume (Fig. 2f), reduced ocean surface heat content (Fig. 2h), large albedo (Fig. 2i) and soil moisture (Fig. 2j). There is a rapid recovery due to the fact that snow is also absent in the initial state, so that it doesn't amplify the initial cooling. In each of the simulation the first 50 years are characterized by rapid vegetation growth, with the well-known succession of grass and trees also discussed in Braconnot et al (2019) . This first rapid phase is followed by a long-term adjustment related to slow climate-vegetation feedback of about 300 years. As expected, the ocean heat content adjustment has the largest adjustment time scale. The equilibrium state is characterized by multiscale variability. These interannual to multidecadal variability is smaller than the differences between the experiments, but need to be accounted for to properly discussed differences between the simulated climatologies. A conclusion from Fig. 1 is that 300 years of simulation is a minimum length to properly analyze the difference between the simulations, which is consistent with the adjustment time reported by Braconnot et al. (2019). It justifies our choice to save computing time by considering simulations from 400 to 1000 year depending on the experiment.

FIG.2

3 Simulated changes between mid-Holocene and pre-industrial climates

3.1 Temperature and precipitation changes

We first focus on the mid Holocene changes simulated by the four versions of the model, using the simulated preindustrial climate as a reference. The major differences between the model versions are well depicted in Fig. 3 considering only annual mean surface air temperature and precipitation for the V3 and V4 model versions. During mid-Holocene the large Earth's axial axis tilt induces a slight reduction of incoming solar radiation in the tropics and an increase in high latitudes. This effect is further amplified (or damped) by the fact that, during mid-Holocene, Earth's precession enhances the insolation seasonality in the northern hemisphere and decreases it in the southern hemisphere (COHMAP-Members, 1988). The annual mean reflects thus both the annual mean change in insolation

https://doi.org/10.5194/egusphere-2024-4075
Preprint. Discussion started: 22 January 2025

and the large seasonal changes and the associated atmospheric, oceanic and land surface feedbacks. It is characterized by an annual mean warming in mid and high latitudes in the northern hemisphere and annual mean cooling in the southern hemisphere (Fig. 3). The annual mean cooling in the tropics over land is a fingerprint of enhanced boreal summer monsoon (Joussaume et al., 1999). The latter is driven by dynamical effects that deplete precipitation over the ocean and increase it over land (Braconnot et al., 2007; D'Agostino et al., 2019). These results are consistent with those of the multimodel ensemble of PMIP mid-Holocene simulations (Brierley et al., 2020). They cover a large fraction of the spread of temperature changes produced by different models worldwide (Brierley et al., 2020), stressing that cascading feedbacks induce by dynamical vegetation have profound impact on regional climate characteristics.

FIG. 3

The results of the different model versions are compared in Fig. 4 to those of the standard IPSL model without dynamical vegetation and the climate reconstructions from pollen and macrofossils data by Bartlein et al. (2011). These diagnoses complete the maps presented in Fig. 3 by indicating that the largest annual mean warming in mid and high latitude is found for V2, and that for most of the boxes V2 simulated changes in temperature and precipitation are not statistically different from those simulated with V3 when accounting for uncertainties between 100-year averages (Fig. 5). The results obtained with the version V4 are the closest to the those obtained with standard IPSLCM6 version of the model used for PMIP4 mid-Holocene simulations. They appear to be in overall better agreement with climate reconstructions. All versions with dynamical vegetation produce larger changes in West Africa, as it is expected with vegetation feedback. The spread between the different 100 years differences between the mid-Holocene and preindustrial climate for a given model version also stresses that long term variability induces uncertainties in 100-year estimates of about 0.5 to 3 °C depending on the region. This needs to be accounted for since 100-year variability can be as high as the signal in some places.

FIG. 4

3.2 Land surface feedbacks between mid-Holocene and preindustrial climates

These differences between the model versions come from the various feedbacks induce by the different changes in the land-surface model and feedbacks induced by the dynamical vegetation. We synthesize the mid-Holocene differences with preindustrial by showing the mean root mean square difference between the two climates in Fig. 5 for leaf area index (*lai*), snow, and atmospheric water content. These diagnoses allow to account both for the differences in the annual mean and in seasonality arising in response to annual mean changes in insolation between the mid Holocene and the preindustrial climates. In order to also account for the centennial variability, we use all possible combinations of 100-year annual mean cycles differences between the two periods for these rms estimates, neglecting the first 300 years of each simulation. For a given variable var in simulation 1 (*var1*) and simulation 2 (*var2*) the rms is thus computed as:

$$rms(var) = \sqrt{\frac{1}{n_1 \times n_2} \sum_{i=4}^{n_1} \sum_{j=4, j\geq i}^{n_2} \sum_{m=1}^{12} (var1 - var2)^2} \quad (2)$$

https://doi.org/10.5194/egusphere-2024-4075
Preprint. Discussion started: 22 January 2025

where n_1 and n_2 represent the number of non-overlapping 100 years in simulation 1 and 2 respectively (and neglecting n = 1 to 3 for the first 300 years), and m refers to months, with 1 being the first month of the year and 12 the last month. The dispersion between the 100-year estimates provides a measure of the uncertainty. We only discuss in the following aspects that are statistically significant.

The *lai* rms between mid-Holocene and preindustrial climates (Fig. 5a to d) highlights that almost all regions have change in vegetation (*lai*) at the mid Holocene compared to preindustrial. This is found with all four model versions. It also shows that regions that experience the largest changes are the Sahel Sahara, northern India, Eurasia and the eastern part of North America, although the magnitude and regional details depend on the model version. The large *lai* changes in Africa highlight that all of these model versions produce a green Sahara which was not the case with the previous versions of the IPSL model (Braconnot et al., 2019). These is consistent with the increased annual mean precipitation and decrease in temperature (Fig. 3). Note that this large amplification couldn't be anticipated from the standard PMIP4-CMIP6 simulation where vegetation is prescribed to preindustrial vegetation, even though changes in monsoon rainfall were larger than with previous IPSL model version (Braconnot et al., 2021). It results from vegetation feedbacks amplified by synergy with ocean feedbacks (Braconnot et al., 1999), and from atmospheric physics and land surface improvement between the IPSLCM5 and IPSLCM6 versions of the IPSL model (Boucher et al., 2020; Hourdin et al., 2020).

FIG. 5

Model versions producing the largest annual mean temperature changes in Eurasia and eastern north America are also those (V3 and V4) producing the largest changes in *lai* (Fig. 5). The snow *rms* indicates that these regions coincide with regions having the largest changes in snow cover (reduced snow cover during mid-Holocene). It is more pronounced for the two model versions (V2 and V3) with the largest temperature changes. This is the footprint of a direct feedback loop between vegetation temperature and snow cover, which further triggers temperature changes due to its large surface albedo. Mid-Holocene temperature, snow and sea-ice changes also induce substantial differences in the atmospheric water content, with largest differences arising within the tropical regions (Fig. 5). Again, the two model versions (V2 and V3) with the largest temperature changes produce the largest changes in atmospheric water content (Fig. 5 right (i) to (l), right column). These model versions also have the largest changes in sea-ice between the two periods and thereby of water vapor in the north Atlantic.

3.3 Estimations of the radiative feedbacks between mid-Holocene and preindustrial climates

We further estimate the radiative feedbacks (Fig. 6). We quantify the shortwave (SW) radiative impact of surface albedo, atmospheric diffusion and scattering on the Earth radiative budget at the top of the atmosphere using the simplified method developed by Taylor et al. (2007). It consists in estimating the integral properties of the atmosphere (scattering, diffusion) and the footprint of the surface albedo on the top of the atmosphere shortwave radiations for the different climates. Following Braconnot et al. (2021), we first estimate for each simulation the atmospheric absorption μ as:

$$\mu = \alpha_p \left({}^{SWsi}/_{SWi} \right)(1 - \alpha_p) \quad (3),$$

https://doi.org/10.5194/egusphere-2024-4075
Preprint. Discussion started: 22 January 2025

and the atmospheric scattering γ as:

$$\gamma = \frac{\mu - (SWsi/_{SWi})}{\mu - \alpha_s (SWsi/_{SWi})} \quad (4),$$

where α_p and α_s stand respectively for the planetary and the surface albedos, and SW_i and SW_{si} for the incoming solar radiation at the top of the atmosphere (insolation) and at the surface. The planetary and surface albedos are computed from the downward and upward SW radiations. By replacing one by one the factors obtained for one climate (or one simulation) by those obtained for the other climate (or another simulation) we have access to the radiative effect of this factor between the two climates (or two simulations). As an example, the effect of a change in the surface albedo in simulation 2 compared to simulation 1 used as reference is provided by:

$$\alpha_p(\mu_1, \gamma_1, \alpha_{s_2}) - \alpha_p(\mu_1, \gamma_1, \alpha_{s_1}) \quad (5)$$

The decomposition done for short wave radiation is not valid for long wave (LW) radiation (Taylor et al., 2007). However, in the case of the simulations considered here we can assume that the LW forcing due to trace gazes is small (Braconnot et al., 2012; Otto-Bliesner et al., 2017). The mid Holocene change in outgoing longwave radiation at the top of the atmosphere (TOA) corresponds thus to the total LW radiative feedbacks. The outgoing long wave at TOA is composed of two terms, the surface outgoing longwave radiation ($LWsup \sim \sigma T^4$, where σ is the Stefan-Bolzmann constant) associated to the surface and the atmospheric atmospheric heat gain ($LW_{sup} - LW_{TOA}$) resulting from the combination of changes in atmospheric water vapor, clouds and lapse rate. The relative magnitude of these different terms cannot be estimated here.

FIG. 6

We focus for this feedback quantification on the mid to high latitudes between 45° N and 80° N where differences in *lai* and in snow cover are the largest between the mid-Holocene and the preindustrial climates between the simulations (Fig. 6). The V2 and V3 versions of the model produce feedbacks as large as the forcing, except it is maximum in boreal spring when the forcing is maximum in summer and early autumn. The dominant factor to amplify the insolation forcing is the land surface albedo (Fig. 6b). It results from the combination of vegetation and snow changes, with a dominant effect of snow because of its larger albedo. The snow albedo effect is amplified when grass is replaced by forest in the mid-Holocene simulation, which occurs over a large area in Eurasia for V2 and V3 compared to V1 where grass is dominant or V4 where a larger fraction of forest is still present in the preindustrial simulation (Fig. 7). Feedbacks in LW radiation have also a large impact in modifying the top of the atmosphere total radiative fluxes. It reduces the effect of the albedo feedback by allowing more heat to escape to space. Interestingly, the direct surface temperature effect (Planck) is partly compensated by an increased greenhouse gas effect resulting from increased water vapor and change in atmospheric lapse rate, in places where the surface warming is maximum (Fig. 3 and Fig. 5).

FIG. 7

4 Differences between model versions and dependence of radiative feedback to climate mean state

The first order feedbacks highlighted between vegetation, temperature, snow and albedo in previous section have different magnitude depending on the model versions (Fig. 6). They arise from differences in model content and

https://doi.org/10.5194/egusphere-2024-4075
Preprint. Discussion started: 22 January 2025

first-order albedo and water vapor feedbacks, some of which may mask the initial effect due to model content. We thus investigate if we can attribute some of the systematic differences in climate and vegetation cover to the different parameterizations and tuning of bares soil evaporation, photosynthesis or pft 7 and 8 critical temperature.

4.1 Systematic differences between model versions for the mid-Holocene

The successive model developments were targeted to produce mid-Holocene boreal forest as the dominant pfts further north in Eurasia and north America when going from the V1 to the V4 versions of the model (Fig. 7). Considering only the dominant pft in Fig. 7 masks the fact that vegetation is represented by a mosaic of 15 pfts in each model grid box. We present in Fig. 8 the global vegetation assemblages of the 15 pfts in order to better highlight the differences between the simulations. It reflects the major differences found at regional scales. As expected from model developments, major differences between the simulations are found for pft 7 (Boreal Needleleaf Evergreen) for the mid-Holocene (Fig. 8a). It represents about 5-10% of the total vegetation cover in V1 and V2 and 13% in V2 and V4. In V2, pft 9 (Boreal Needleleaf Deciduous) is the dominant type of boreal forest (9% of total vegetation cover), while in V1, boreal forest is poorly represented.

FIG. 8

All model versions, except V1, use *barenew* parameterization for bare soil evaporation. It appears to be a critical model aspect contributing to a better representation of boreal forest. Bare soil evaporation is small in all simulation except V1 where it peaks in May-June (Fig. 9a), at a time when tree leaves are growing in the northern hemisphere and soils are saturated. With the *bareold* parameterization the evaporation in these conditions is close to potential evaporation. The other simulations do not produce the large boreal spring bare soil evaporation, due to the fact that evaporation is limited by soil and biomass characteristics (see Section 2.1). In these simulations, the evapotranspiration is slightly larger and peaks in July-August at the time of the maximum development of vegetation in the northern hemisphere (Fig. 9a). Statistically significant higher values are found for V4 which is also the warmest simulation. As a result, surface soil moisture is larger in V2 to V4 compared to V1, and favors tree growth. Interestingly the total evaporation remains almost the same between all simulations but the surface soil moisture is higher in V3 to V4 compared to V1 (Fig. 9c).

FIG. 9

Large differences are also found in the distribution between the different grass pfts between the mid Holocene simulations, V1 having the largest proportion of pft 10 and 14, which results and contribute to the fact that this simulation is the coldest one with the largest snow cover (Fig. 9b). The partitioning between grass and tree leads to different magnitude in soil moisture between the simulations, associated to difference in root depths and to the way these different types of vegetation recycle water. It affects temperature through evaporative cooling and the amplification of the surface albedo by snow in mid and high latitude. The differences in the surface albedo and the different linkages between snow and vegetation are well depicted in Fig. 10 (a) for the 45°N-80°N region. The large difference found between the simulations for albedos in the range 0.3 to 0.7 is the footprint of the difference in the ratio of tree and grass cover, with grass dominant vegetation for V1 and a mixture of grass and pft 9 for V2.

https://doi.org/10.5194/egusphere-2024-4075
Preprint. Discussion started: 22 January 2025

The peak emerging for albedo around 0.22 in V3 and V4 is related to the pft 7 coverage in these simulations (Fig. 8). It highlights that the overall albedo combination of tree and snow albedo leads to a smaller albedo in these two simulations. All the mid-Holocene simulations have a quite similar coverage of high albedo, which is compatible with similar distribution of sea-ice and regions fully covered by snow. The lower coverage for albedo > 0.7 % is for V4 which has the smaller sea-ice cover.

FIG. 10

In terms of radiative feedbacks between 45° N and 80° N, the surface albedo effect varies significantly between the simulations (Fig. 12a, b). The radiative feedbacks are computed using the Taylor et al. (2009) methodology following what was done for the mid-Holocene differences with the preindustrial climate in section 3.2, except that the V4 version of the model serves as reference. Positive values (negative) indicate that the feedback brings more (less) energy to the climate system in V4. Since we compare the simulations for a given climate, the forcing is the same for all the mid-Holocene simulations, and the only factor affecting the global energy balance comes from differences in seasonal climate feedbacks. The largest differences in surface albedo feedbacks between the V4 and the V1 to V3 versions of the model occur from February to July. It is maximum for V1 due to the largest snow-vegetation albedo feedback, as expected from the distribution of surface albedo between 45° N and 80° N (Fig. 10). This effect exceeds 10 W m^{-2} (up to about 16 W m^{-2}) from April to June. The effect is smaller between V4 and V2 or V3, but with maximum of 10 W m^{-2} for V2 and 8 W m^{-2} for V3. Note that for V2 and V3 the larger radiative effect comes from the albedo combination with the type of boreal forest (pft 7 or pft 9) more than from the relative distribution between grass and forest (Fig. 10).

The cloud SW feedback differences between the simulations slightly amplify the effect of the surface albedo from April to September in V1 to V3 compared to V4 (Fig. 11c). Part of the signal is damped by long wave radiation resulting from temperature, clouds and lapse rate (Fig. 11d). This is mainly due to the differences in evapotranspiration between the mid-Holocene simulations (Fig. 9a) resulting from the combination of vegetation characteristics, but also from differences from the insulating effect of snow and ice cover in mid and high latitudes (Fig. 11). It is strongly tied to temperature, and thereby to the atmospheric water holding capacity. The V4 mid-Holocene simulation has the largest atmospheric water content, with maximum difference with the other simulation in the northern hemisphere (Fig. 12). Despite the fact that the representation of boreal forests and the interactions between vegetation and snow (Fig. 8, and 10) is the major cause of the differences between the simulations, the largest water content differences are found in the tropics, with statistically significant differences found up to 40° S (Fig. 12). It reminds us that, in the fully coupled system, rapid energy adjustment between the hemispheres and between land and ocean are induced by the regional differences in energy sinks and sources, and that these rapid teleconnexions also shape the simulated climate mean state. It also stresses the important role of the tropics and tropical ocean in regulating the global atmospheric moisture, and in balancing solar forcing and SW feedbacks.

FIG. 11

https://doi.org/10.5194/egusphere-2024-4075
Preprint. Discussion started: 22 January 2025

The role of photosynthesis in regulating seasonal feedbacks needs to be highlighted. An example of systematic difference in vegetation cover associated to PhotoCM5 and PhotoCM6 is found in Australia where the dominant pft is forest for V3 and V4, whereas it is grass for V1 and V2. It doesn't affect much the representation of boreal forest which is quite similar between V3 and V4, certainly because the parameter adjustments were done with the aim to allow tree growth for lower temperature than the one used in the standard model version (see section 2.1). At the global scale, despite different distribution of vegetation, the two simulations with PhotoCM5 (V2 and V3) instead of PhotoCM6 (V1 and V4) exhibit a larger *lai* seasonal cycle (Fig. 9e), whatever the realism of the simulated vegetation. In V2 and V3, GPP has a strong increase from March to July when the peak GPP is reached (Fig. 9f). The *lai* seasonality is smoother in V1 and V4. The parallel *lai* seasonal evolution between V1 and V4 reflects a similar behaviour with an offset resulting from differences in temperature and differences in vegetation coverage (in particular for temperate forests). The shape of PhotoCM5 as a function of temperature compared to PhotoCM6 (Fig. 1) favours larger productivity (*gpp*) as soon as *lai* is developing. This means that for given climatic conditions, the start of the growing season should be similar with the two parameterisations, but photoCM5 should have larger *gpp*. This is indeed what we obtained between the simulations (Fig. 9e, f). This systematic difference affects the seasonality of the surface albedo, through the *lai* and the total soil moisture. Reduced *gpp* during the growing season in the northern hemisphere implies more humidity in the soil, as it can be seen on Fig. 9 between V4 and V2 or V3, which are simulations sharing the same bare soil evaporation. Due to all the interactions in the climate system, we also end up with the counter intuitive result that V4 has the largest vegetation cover (Fig. 9), but that the vegetation is less productive than in V3 and even V2.

FIG. 12

4.2 Dependence of vegetation induced radiative feedbacks on mean climate state.

The feedbacks and their seasonal evolution between the model versions discussed for the mid-Holocene are very similar to those occurring between Mid-Holocene and preindustrial climates for each model version. However, the comparison of Fig. 6 and Fig. 11 (a to d) suggest that the strength of the feedback is different between the two periods, which is indeed the case (Fig. 11e to h). It raises questions on the way to compare different periods and use them to investigate non-linear effects and thresholds.

The simulations have all in common consistent changes in vegetation between the mid-Holocene and preindustrial climates (Fig. 7 and 8). At the global scale the larger fraction of bare soil and grasses simulated for the preindustrial climate (Fig. 8) is consistent with the drying of the Sahara Sahel, and the southward retreat of the tree line in the northern hemisphere (Fig. 7). Also, most of the inter model differences in vegetation cover discussed for the mid-Holocene are also found between the simulations of preindustrial climate (Fig. 7 and 8). In particular, this is the case for the representation of the mosaic vegetation at the global scale (Fig. 8b), so that magnitude of change between the two periods for each pft is consistent with the distribution of vegetation for each model version (Fig. 7 and 8). The distribution of vegetation appears thus to first order as a factor characterizing a model version.

However, notable differences are found that have implications on the relative differences between the preindustrial simulations when considering the preindustrial quantification of the 45° N and 80° N SW and LW radiative feedbacks (Fig. 11). It highlights that the sensitivity of the feedback to the climate mean state is higher for model versions with PhotoCM5 rather than PhotoCM6 (Fig. 11). The differences reach up to 20 W m^{-2} in V4 compared to V2 to 25 W m^{-2} in V4 compared to V3. It is in part due to a larger impact of snow albedo (Fig. 10). For example, V3 and V4 have a similar fraction of pft 7 in the mid-Holocene, but not in the pre-industrial climate (Fig. 8). In V3, boreal forest is replaced by a larger fraction of grass (pft 11) and bare soil (pft 1). There is also a larger fraction of grass and bare soil in V2, whereas V1 doesn't change much compared to the mid-Holocene and vegetation is dominated by grass and bare soil (Fig. 8). There is thus a larger fraction of the points where the surface albedo is in the 0.3 to 0.7 range (Fig. 10). Contrary to the mid-Holocene climate, there are also large differences in the 0.7 to 0.9 albedo range characterizing snow and sea-ice between the simulations (Fig. 10b). The largest increase is found for V2 and V3, for which the number of points with low albedo value is also reduces, confirming that it is due to a larger increase in sea-ice cover in these two simulations. For the preindustrial period, all simulation, except V4 have a two large cover of sea-ice over the ocean (not shown) and cold temperatures associated to it. The initial vegetation-albedo feedback is amplified by the sea-ice albedo feedback, which affect temperature, water vapor, and the crossing of different thresholds controlling vegetation growth.

The difference in the seasonal insolation forcing compared to the mid-Holocene induces differences in the shape of the surface albedo feedback in model differences as a function of month, with values that are still large between V4 and V2 or V3 from July to September (Fig. 11b, f). Differences between the two periods are also found in the seasonality of atmospheric scattering (mainly due to clouds), even though the magnitude of the scattering is quite similar to what was obtained for the mid-Holocene (Fig. 11c, g). As for the mid-Holocene, the seasonal insolation and temperature at the beginning of the growing season trigger some of the important differences in the photosynthesis and gpp depending on the photosynthesis parameterization. The major differences in the relationship between *lai* and gpp discussed for the mid-Holocene (Fig. 9e, f) are also found for the preindustrial climate (not shown). However, *lai* is more similar between the V3 and V4 because of larger grass and bare soil fraction in V3, which compensate from the tendency to produce larger *lai*. The difference in vegetation growth between V3 and V4 is controlled by the critical threshold for tree mortality and the shape of the photosynthesis curve. Compared to the mid-Holocene climate, less insolation is received in mid and high latitude during boreal summer. For both climates the simulation using PhotoCM5 is colder. Therefore, the surface temperature is closer to the *tcrit* value in Spring in this simulation, compare to the simulation using PhotoCM6. It induces a larger reduction of the tree cover and of *lai* and *gpp* (not shown), In contrast, the pre-industrial vegetation growth follows the seasonal insolation forcing as for the mid-Holocene climate with PhotoCM6. This result implies that the sensitivity of the seasonal vegetation feedback is a critical factor that needs to be properly constraint to reduce uncertainties in radiative feedbacks and vegetation-climate interactions and associated cascading effects.

The cascading effects involve the LW radiative feedback and its linkages with temperature (Fig. 11h). The larger longwave radiative feedback in V4 is accompanied by a larger atmospheric heat gain to compensate for the larger shortwave radiative feedback compared to the mid-Holocene (Fig. 10). As for the mid Holocene, the atmospheric water vapor heat content is larger for V4 compared to the other simulations with larger differences found in the tropics and in the northern hemisphere. The amplification in the atmospheric water content in northern hemisphere reflect the differences in sea-ice cover and thereby evaporation over the ocean. Interestingly the difference in

https://doi.org/10.5194/egusphere-2024-4075
Preprint. Discussion started: 22 January 2025

atmospheric water content is similar in the preindustrial and mid-Holocene simulations between V4 and V1 whereas it is a factor 2 in the preindustrial compared to the mid-Holocene between V4 and V2 or V3. It is clearly tied to the amplitude of vegetation changes and sea-ice feedback. The large differences in annual mean temperature in mid and high latitude between the mid-Holocene and preindustrial climates simulated with the different version of the model (Fig. 3) come thus for a large part from the simulations of the preindustrial climate.

5 Discussion and conclusion

The suite of mid-Holocene and preindustrial climate simulations considered here allow us to dig into the complexity of the Earth's climate system. We insist on the fact that climate-vegetation interactions induce seasonal feedbacks that trigger unavoidable first order albedo and water vapor radiative feedbacks. A full understanding and thereby the ability to improve Earth's system model simulations requires studying these feedbacks in the fully coupled system. Indeed, the climate mean characteristics is related to the relative contributions of SW and LW radiative feedbacks that are needed to balance the top of the atmosphere radiative budget depending on the forcing. These feedbacks do not necessarily occur where changes occur on the land surface, but remotely, as it is the case for the water vapor in this study, which is maximum in the tropical regions when major snow-ice-vegetation albedo feedbacks are maximum in mid and high northern latitudes (Fig. 5 and Fig. 11). The LW radiative feedback is less discussed when the role of vegetation is inferred from vegetation alone simulations or simulations where the sea surface temperature and sea-ice cover are prescribed. It is a first order effect associate to the change in temperature and fulfil the convective radiative equilibrium which serves as a basis for the reasoning on climate sensitivity (Dufresne and Bony, 2008; Manabe and Wetherald, 1975; Sherwood et al., 2020). It is often neglected also because it is maximum over the ocean and in the tropics, which is in general not part of the focus when analysing vegetation over land.

FIG. 13

We show that dynamical vegetation reveals how the land surface and seasonal evolution of vegetation trigger atmospheric feedbacks, considering the mid-Holocene and the preindustrial climates. The comparison of two periods that have no difference in annual global mean forcing, but difference in seasonality induced by Earth's orbit provides an efficient way to investigate the role of the vegetation seasonal feedbacks and how they are affected by bare soil evaporation, photosynthesis and temperature threshold for boreal tree mortality. It also allows to investigate the sensitivity of vegetation feedbacks to the mean state dependence. We synthetize the results considering global annual mean in Fig. 13. At the global scale the warmest mid-Holocene simulation is the one run with V4. There is almost 1 °C difference with the coldest simulations, V1. As expected from the Clausius Clapeyron relationship, since the atmospheric and oceanic physics are the same between the model versions, the warmest simulation is also the simulation with the highest atmospheric water content. The warmest simulation has also the smallest snow and sea-ice cover (Fig 13d, e). The step changes between the model version for snow cover and sea-ice cover is different from the one in temperature or atmospheric water content, which we attribute to the fact that the seasonal vegetation-albedo feedback depends on the mosaic vegetation and its associated *lai* and productivity (Fig. 13f to k).

https://doi.org/10.5194/egusphere-2024-4075
Preprint. Discussion started: 22 January 2025

Model content and vegetation-climate temperature interactions lead to different vegetation cover, with maximum difference in the representation of gasses, temperate and boreal forest for the mid-Holocene simulations (Fig. 13). Our results show that the warmest simulation is not necessarily the one with the largest *lai* and productivity. The latter are mainly driven by the choice of the photosynthesis parameterisation (section 4). The climate state dependence of the seasonal feedbacks is also driven by the differences in the photosynthesis parameterisation. The parameterisation, and the way it triggers vegetation growth and gpp, regulate the strength of the snow-vegetation feedbacks and its functioning when temperature reaches the threshold temperature for tree mortality. This is independent of the exact representation of the vegetation cover. Differences in the magnitude of the seasonal feedbacks leads to different directions in the global annual mean temperature values between mid-Holocene and preindustrial periods. Vegetation cover is reduced in the preindustrial climate compared to the mid-Holocene, which is a well-known fact (Bigelow et al., 2003; Jolly et al., 1998; Prentice et al., 1996). However, depending on the choice of the photosynthesis parameterisation *lai* and *gpp* are reduced or slightly increased in the preindustrial (Fig. 13k, l), which characterises a larger seasonal sensitivity for photoCM5 than photoCM6. Vegetation feedbacks are such that the global mean temperature is reduced with photoCM5, and the increase of snow and sea-ice cover is larger. Temperature is slightly increased, and global snow cover similar to mid-Holocene with photoCM6 and sea-ice slightly increased. The sea-ice and snow feedbacks are first triggered by the seasonal insolation forcing, but are amplified by land-surface climate interactions. The bare soil evaporation doesn't affect the direction of the annual mean changes between mid-Holocene and preindustrial climates. It has a major impact on the tree cover, and thereby on temperature though snow-vegetation-evaporation feedback.

Our results confirm that the simulated vegetation is an integrator of the seasonal feedbacks and is fully representative of the climate annual mean state. This result is somehow trivial since it is in full agreement with the definition of climate in geography that involve the linkage between weather and environment. It is valid between climates, but also between simulations run with different model versions (Fig. 7 and Fig. 8). Dynamical vegetation is thus a key factor to consider to infer the realism of vegetation feedback in the climate system. These feedbacks cannot be fully inferred from simulations where vegetation is prescribed. In addition, our results point to important differences induced by photosynthesis that can only be assessed in the fully coupled system. They also indicate that seasonal feedbacks have a key impact on climate changes. Paleoclimate periods for which the major difference with present day come from the annual cycle of the insolation forcing such as the mid-Holocene or the last interglacial periods considered as part of PMIP (Kageyama et al., 2018; Otto-Bliesner et al., 2017) are well-suited to provide observational constraint on these feedbacks, even when indirectly from seasonal information on temperature, precipitation, sea-ice cover, or from vegetation.

The global annual differences between the simulations are small, even though statistically significant, and comes from differences in the simulated climate annual mean cycle. It stresses that a proper evaluation of climate variables cannot be properly infer from annual mean values, and that specific time in the year when key feedback occur need to be targeted in order to go one step further. This is certainly also true for climate reconstructions. Depending on the method and records considered, substantial differences are found in annual mean reconstruction for the mid-Holocene climate (Brierley et al. 2020). The choice of records and physical or biogeochemical variable should thus be chosen depending on the feedback or process considered. Our results also highlight that considering multi-

https://doi.org/10.5194/egusphere-2024-4075
Preprint. Discussion started: 22 January 2025

decadal to centennial variability is needed because it can be high in some regions or simulations. This has been discussed for a long time for paleoclimate simulations (Hewitt and Mitchell, 1996; Otto et al., 2009a), but model groups tend still to only provide simulations with limited length when contributing to the PMIP database for model-intercomparison (Brierley et al., 2020). This might lead to erroneous model ranking or interpretation of model differences in some cases.

The reference period chosen to evaluate the results of the simulated vegetation is also an issue. In this study, we show that differences between the model version in the simulation of mid-Holocene climate and vegetations changes come mainly from the simulation of the preindustrial climate. Indeed, differences are larger between the simulations of the pre-industrial climate than between the simulations of the mid-Holocene climate. Direct comparison of the mid-Holocene climate, and not the differences with pre-industrial, would be required, as well as differences between different climate periods, to fully infer the realism of the simulated climate. This is a direction to consider for future research that would help better infer the ability of a model to simulate the annual mean cycle. The reference period is also an issue to evaluate the simulated vegetation. We directly develop the model version using simulations of the mid-Holocene climate. The V3 and V4 version of the model appears to be rather equivalent with respect to the simulated vegetation, except that a full evaluation was not done. This would requires transforming the 15 simulated pft into the equivalent biomes inferred from pollen (Prentice et al., 1996) which was out of the scope of this paper and also introduce artificial choices (Braconnot et al., 2019; Dallmeyer et al., 2019). It is also difficult to compare the preindustrial simulations with preindustrial vegetation maps, because land used is not considered in these simulations. Land use has also an indirect impact on the simulated natural vegetation through its effect on temperature and evapotranspiration. An attempt to evaluate the simulated vegetation is provided on Fig. 9 by considering only grid points for which there is no land use in the preindustrial climate. The stars on the figure correspond to the fraction occupied by each pft for the V4 version and the reference 1850 vegetation map used when vegetation is prescribed to the model, as it is the case for CMIP6 preindustrial simulations (Boucher et al., 2020). It suggests that, for the preindustrial climate, this last version of the model overestimates the fraction of tropical forest (mainly pft 3), has a reasonable representation of temperate forest (pft 4 to 6), overestimates boreal forest (mainly pft 7), and has a reasonable representation of grass, with the caveat that there is a misbalance between pft 15 and pft 11. Overall it is quite reasonable and better than in the other versions (not shown). This model version has been retained for transient Holocene simulations with the IPSL model and dynamic vegetation.

FIG. 14

Our results have also implications for the land-surface carbon feedbacks and the representations of the interactions between energy, water and carbon cycle in Earth system models. Here the carbon dioxide concentration is prescribed in the atmosphere, but the carbon cycle is activated, so that carbon fluxes between the surface and the atmosphere can be diagnosed. The pattern and magnitude are model version dependent. Figure 14 illustrates the differences that are found between the mid-Holocene and the preindustrial climates, considering the V3 and V4 version of the model. As expected, the differences induced by the photosynthesis on *gpp* and climate lead to significant differences in the mid-Holocene change in carbon fluxes over land. It would lead to differences in regional

https://doi.org/10.5194/egusphere-2024-4075
Preprint. Discussion started: 22 January 2025

and global carbon concentration in the atmosphere if carbon was fully interactive, and thereby certainly to different climate and vegetation characteristics. This need further investigation. It also stresses that further emphasize on seasonality is needed to better assess land-surface feedbacks and the way they trigger the first order albedo and water vapor radiative feedbacks. Clouds certainly need to be also considered. They are key component and a major source of uncertainty when considering different climate models with different atmospheric physics, but are of an order of magnitude smaller that the other two feedbacks and their uncertainties when considering only the linkages with seasonal vegetation feedbacks, as it is the case here.

Finally, a further implication of this study it that dynamical vegetation is an important factor in the climate system and should be considered in Earth System Model (i.e. climate models with interactive carbon cycle). simulations used to investigate possible futures if one which so properly account for the way land surface triggers cascading feedback effects in a changing climate. This also means more degrees of freedom in the system, and thereby to potentially larger model biases or uncertainties despite more accurate representation of internal processes.

Data availability: All data used to produce the different figures have been posted on the FAIR repository under https://doi.org/10.5281/zenodo.14536307.

Author contribution: All authors contributed to the experimental design. PB and NV developed and implemented the necessary changes to the land surface model. PB developed and run the coupled simulations. PB and OM performed the analyses of the coupled simulations. All authors contributed to the drafting of the manuscript.

Competing interests: The authors declare that they have no conflict of interest.

Acknowledgements. It benefits from the development of the common modeling IPSL infrastructure coordinated by the IPSL climate modeling center (https://cmc.ipsl.fr). Data files were prepared with NCO (NetCDF Operators; Zender, 2008, and http://nco.sourceforge.net). Maps were drawn with pyFerret, a product of NOAA's Pacific Marine Environmental Laboratory (http://ferret.pmel.noaa.gov/Ferret,). Other plots are produced with PyFerret or with Matplotlib (Hunter, 2007, and https://matplotlib.org) in Jupyter Python notebooks.

Financial support: We acknowledge the project TipESM "Exploring Tipping Points and Their Impacts Using Earth System Models". TipESM is funded by the European Union. Grant Agreement number: 101137673. DOI: 10.3030/101137673. Contribution nr. 6. This work was granted access to the HPC resources of TGCC under the allocations A0170112006, A0150112006, A0130112006, and A0110112006 made by GENCI.

References

Arias, P. A., Bellouin, N., Coppola, E., Jones, R. G., Krinner, G., Marotzke, J., Naik, V., Palmer, M. D., Plattner, G.-K., Rogelj, J., Rojas, M., Sillmann, J., Storelvmo, T., Thorne, P. W., Trewin, B., Achuta Rao, K., Adhikary, B., Allan, R. P., Armour, K., Bala, G., Barimalala, R., Berger, S., Canadell, J. G., Cassou, C., Cherchi, A., Collins, W., Collins, W. D., Connors, S. L., Corti, S., Cruz, F. A., Dentener, F. J., Dereczynski, C., Di Luca, A., Diongue-Niang, A., Doblas-Reyes, F. J., Dosio, A., Douville, H., Engelbrecht, F., Eyring, V., Fischer, E., Forster, P., Fox-Kemper, B., Fuglestvedt, J. S., Fyfe, J. C., Gillett, N. P., Goldfarb, L., Gorodetskaya, I., Gutiérrez, J. M., Hamdi, R., Hawkins, E., Hewitt, H. T., Hope, P., Islam, A. S., Jones, C., Kaufman, D. S., Kopp, R. E., Kosaka, Y., Kossin, J., Krakovska, S., Lee, J.-Y., Li, J., Mauritsen, T., Maycock, T. K., Meinshausen, M., Min, S.-K., Monteiro, P. M. S., Ngo-Duc, T., Otto, F., Pinto, I., Pirani, A., Raghavan, K., Ranasinghe, R., Ruane, A. C., Ruiz, L., Sallée, J.-B., Samset, B. H., Sathyendranath, S., Seneviratne, S. I., Sörensson, A. A., Szopa, S., Takayabu, I., Treguier, A.-M., van den Hurk, B., Vautard, R., von Schuckmann, K., Zaehle, S., Zhang, X., and Zickfeld, K.: Techincal summary, in: Climate Change 2021: The Physical Science Basis. Contribution of Working Group I to the Sixth Assessment Report of the Intergovernmental Panel on Climate Change, edited by: Masson-Delmotte, V., Zhai, P., Pirani, A., Connors, S. L., Péan, C., Berger, S., Caud, N., Chen, Y., Goldfarb, L., Gomis, M. I., Huang, M., Leitzell, K., Lonnoy, E., Matthews, J. B. R., Maycock, T. K., Waterfield, T., Yelekçi, O., Yu, R., and Zhou, B., Cambridge University Press, 33–144, https://doi.org/10.1017/9781009157896.002, 2021.

Aumont, O., Ethé, C., Tagliabue, A., Bopp, L., and Gehlen, M.: PISCES-v2: an ocean biogeochemical model for carbon and ecosystem studies, Geosci. Model Dev., 8, 2465–2513, https://doi.org/10.5194/gmd-8-2465-2015, 2015.

Ball, J. T., Woodrow, I. E., and Berry, J. A.: A Model Predicting Stomatal Conductance and its Contribution to the Control of Photosynthesis under Different Environmental Conditions, in: Progress in Photosynthesis Research, Springer Netherlands, Dordrecht, 221–224, https://doi.org/10.1007/978-94-017-0519-6_48, 1987.

Bartlein, P. J., Harrison, S. P., Brewer, S., Connor, S., Davis, B. A. S., Gajewski, K., Guiot, J., Harrison-Prentice, T. I., Henderson, A., Peyron, O., Prentice, I. C., Scholze, M., Seppa, H., Shuman, B., Sugita, S., Thompson, R. S., Viau, A. E., Williams, J., and Wu, H.: Pollen-based continental climate reconstructions at 6 and 21 ka: a global synthesis, Clim. Dyn., 37, 775–802, https://doi.org/10.1007/s00382-010-0904-1, 2011.

Bigelow, N. H., Brubaker, L. B., Edwards, M. E., Harrison, S. P., Prentice, I. C., Anderson, P. M., Andreev, A. A., Bartlein, P. J., Christensen, T. R., Cramer, W., Kaplan, J. O., Lozhkin, A. V., Matveyeva, N. V., Murray, D. F., McGuire, A. D., Razzhivin, V. Y., Ritchie, J. C., Smith, B., Walker, D. A., Gajewski, K., Wolf, V., Holmqvist, B. H., Igarashi, Y., Kremenetskii, K., Paus, A., Pisaric, M. F. J., and Volkova, V. S.: Climate change and Arctic ecosystems: 1. Vegetation changes north of 55 degrees N between the last glacial maximum, mid-Holocene, and present, J. Geophys. Res.-Atmospheres, 108, 2003.

Boucher, O., Servonnat, J., Albright, A. L., Aumont, O., Balkanski, Y., Bastrikov, V., Bekki, S., Bonnet, R., Bony, S., Bopp, L., Braconnot, P., Brockmann, P., Cadule, P., Caubel, A., Cheruy, F., Codron, F., Cozic, A., Cugnet, D., D'Andrea, F., Davini, P., de Lavergne, C., Denvil, S., Deshayes, J., Devilliers, M., Ducharne, A., Dufresne, J.-L., Dupont, E., Éthé, C., Fairhead, L., Falletti, L., Flavoni, S., Foujols, M.-A., Gardoll, S., Gastineau, G., Ghattas, J., Grandpeix, J.-Y., Guenet, B., Guez, L., Guilyardi, E., Guimberteau, M., Hauglustaine, D., Hourdin, F., Idelkadi, A., Joussaume, S., Kageyama, M., Khodri, M., Krinner, G., Lebas, N., Levavasseur, G., Lévy, C., Li, L., Lott, F., Lurton, T., Luyssaert, S., Madec, G., Madeleine, J.-B., Maignan, F., Marchand, M., Marti, O., Mellul, L., Meurdesoif, Y., Mignot, J., Musat, I., Ottlé, C., Peylin, P., Planton, Y., Polcher, J., Rio, C., Rochetin, N., Rousset, C., Sepulchre, P., Sima, A., Swingedouw, D., Thiéblemont, R., Traore, A. K., Vancoppenolle, M., Vial, J., Vialard, J., Viovy, N., and Vuichard, N.: Presentation and Evaluation of the IPSL-CM6A-LR Climate Model, J. Adv. Model. Earth Syst., 12, e2019MS002010, https://doi.org/10.1029/2019ms002010, 2020.

Braconnot, P. and Kageyama, M.: Shortwave forcing and feedbacks in Last Glacial Maximum and Mid-Holocene PMIP3 simulations, Phil Trans R Soc A, 373, 20140424, 2015.

Braconnot, P., Joussaume, S., Marti, O., and de Noblet, N.: Synergistic feedbacks from ocean and vegetation on the African monsoon response to mid-Holocene insolation, Geophys Res Lett, 26, 2481–2484, 1999.

Braconnot, P., Otto-Bliesner, B., Harrison, S., Joussaume, S., Peterchmitt, J. Y., Abe-Ouchi, A., Crucifix, M., Driesschaert, E., Fichefet, T., Hewitt, C. D., Kageyama, M., Kitoh, A., Laine, A., Loutre, M. F., Marti, O., Merkel, U., Ramstein, G., Valdes, P., Weber, S. L., Yu, Y., and Zhao, Y.: Results of PMIP2 coupled simulations of the Mid-Holocene and Last Glacial Maximum - Part 1: experiments and large-scale features, Clim. Past, 3, 261–277, https://doi.org/10.5194/cp-3-261-2007, 2007.

Braconnot, P., Harrison, S. P., Kageyama, M., Bartlein, P. J., Masson-Delmotte, V., Abe-Ouchi, A., Otto-Bliesner, B., and Zhao, Y.: Evaluation of climate models using palaeoclimatic data, Nat. Clim. Change, 2, 417–424, https://doi.org/10.1038/nclimate1456, 2012.

Braconnot, P., Zhu, D., Marti, O., and Servonnat, J.: Strengths and challenges for transient Mid- to Late Holocene simulations with dynamical vegetation, Clim Past, 15, 997–1024, https://doi.org/10.5194/cp-15-997-2019, 2019.

Braconnot, P., Albani, S., Balkanski, Y., Cozic, A., Kageyama, M., Sima, A., Marti, O., and Peterschmitt, J.-Y.: Impact of dust in PMIP-CMIP6 mid-Holocene simulations with the IPSL model, Clim. Past, 17, 1091–1117, https://doi.org/10.5194/cp-17-1091-2021, 2021.

Brierley, C. M., Zhao, A., Harrison, S. P., Braconnot, P., Williams, C. J. R., Thornalley, D. J. R., Shi, X., Peterschmitt, J. Y., Ohgaito, R., Kaufman, D. S., Kageyama, M., Hargreaves, J. C., Erb, M. P., Emile-Geay, J., D'Agostino, R., Chandan, D., Carré, M., Bartlein, P. J., Zheng, W., Zhang, Z., Zhang, Q., Yang, H., Volodin, E. M., Tomas, R. A., Routson, C., Peltier, W. R., Otto-Bliesner, B., Morozova, P. A., McKay, N. P., Lohmann, G., Legrande, A. N., Guo, C., Cao, J., Brady, E., Annan, J. D., and Abe-Ouchi, A.: Large-scale features and evaluation of the PMIP4-CMIP6 midHolocene simulations, Clim Past, 16, 1847–1872, https://doi.org/10.5194/cp-16-1847-2020, 2020.

Cheruy, F., Ducharne, A., Hourdin, F., Musat, I., Vignon, É., Gastineau, G., Bastrikov, V., Vuichard, N., Diallo, B., Dufresne, J., Ghattas, J., Grandpeix, J., Idelkadi, A., Mellul, L., Maignan, F., Ménégoz, M., Ottlé, C., Peylin, P., Servonnat, J., Wang, F., and Zhao, Y.: Improved Near-Surface Continental Climate in IPSL-CM6A-LR by Combined Evolutions of Atmospheric and Land Surface Physics, J. Adv. Model. Earth Syst., 12, https://doi.org/10.1029/2019MS002005, 2020.

Claussen, M. and Gayler, V.: The greening of the Sahara during the mid-Holocene: results of an interactive atmosphere-biome model, Glob. Ecol. Biogeogr. Lett., 6, 369–377, 1997.

COHMAP-Members: Climatic changes of the last 18,000 years: observations and model simulations, Science, 241, 1043–1052, 1988.

Collatz, G., Ribas-Carbo, M., and Berry, J.: Coupled Photosynthesis-Stomatal Conductance Model for Leaves of C4 Plants, Aust. J. PLANT Physiol., 19, 519–538, https://doi.org/10.1071/PP9920519, 1992.

Craig, A., Valcke, S., and Coquart, L.: Development and performance of a new version of the OASIS coupler, OASIS3-MCT_3.0, Geosci. Model Dev., 10, 3297–3308, https://doi.org/10.5194/gmd-10-3297-2017, 2017.

D'Agostino, R., Bader, J., Bordoni, S., Ferreira, D., and Jungclaus, J.: Northern Hemisphere Monsoon Response to Mid-Holocene Orbital Forcing and Greenhouse Gas-Induced Global Warming, Geophys. Res. Lett., 46, 1591–1601, https://doi.org/10.1029/2018gl081589, 2019.

Dallmeyer, A., Claussen, M., and Brovkin, V.: Harmonising plant functional type distributions for evaluating Earth system models, Clim Past, 15, 335–366, https://doi.org/10.5194/cp-15-335-2019, 2019.

https://doi.org/10.5194/egusphere-2024-4075
Preprint. Discussion started: 22 January 2025

Dallmeyer, A., Claussen, M., Lorenz, S. J., Sigl, M., Toohey, M., and Herzschuh, U.: Holocene vegetation transitions and their climatic drivers in MPI-ESM1.2, Clim. Past, 17, 2481–2513, https://doi.org/10.5194/cp-17-2481-2021, 2021.

Dallmeyer, A., Kleinen, T., Claussen, M., Weitzel, N., Cao, X., and Herzschuh, U.: The deglacial forest conundrum, Nat. Commun., 13, 6035, https://doi.org/10.1038/s41467-022-33646-6, 2022.

Ducharnes, A., Ottlé, C., Maignan, F., Vuichard, N., Ghattas, J., Wang, F., Peylin, P., Polcher, Guimberteau, M., Maugis, P., Tafasca, S., Tootchi,A., Verhoef, A., and Mizuochi, H.: The hydrol module of ORCHIDEE: scientific documentation [rev 3977] and on, work in progress, towards CMIP6v1, 2018.

Dufresne, J. L., Foujols, M. A., Denvil, S., Caubel, A., Marti, O., Aumont, O., Balkanski, Y., Bekki, S., Bellenger, H., Benshila, R., Bony, S., Bopp, L., Braconnot, P., Brockmann, P., Cadule, P., Cheruy, F., Codron, F., Cozic, A., Cugnet, D., de Noblet, N., Duvel, J. P., Ethe, C., Fairhead, L., Fichefet, T., Flavoni, S., Friedlingstein, P., Grandpeix, J. Y., Guez, L., Guilyardi, E., Hauglustaine, D., Hourdin, F., Idelkadi, A., Ghattas, J., Joussaume, S., Kageyama, M., Krinner, G., Labetoulle, S., Lahellec, A., Lefebvre, M. P., Lefevre, F., Levy, C., Li, Z. X., Lloyd, J., Lott, F., Madec, G., Mancip, M., Marchand, M., Masson, S., Meurdesoif, Y., Mignot, J., Musat, I., Parouty, S., Polcher, J., Rio, C., Schulz, M., Swingedouw, D., Szopa, S., Talandier, C., Terray, P., Viovy, N., and Vuichard, N.: Climate change projections using the IPSL-CM5 Earth System Model: from CMIP3 to CMIP5, Clim. Dyn., 40, 2123–2165, https://doi.org/DOI 10.1007/s00382-012-1636-1, 2013.

Dufresne, J.-L. and Bony, S.: An Assessment of the Primary Sources of Spread of Global Warming Estimates from Coupled Atmosphere–Ocean Models, J. Clim., 21, 5135–5144, https://doi.org/10.1175/2008JCLI2239.1, 2008.

Eyring, V., Bony, S., Meehl, G. A., Senior, C. A., Stevens, B., Stouffer, R. J., and Taylor, K. E.: Overview of the Coupled Model Intercomparison Project Phase 6 (CMIP6) experimental design and organization, Geosci Model Dev, 9, 1937–1958, https://doi.org/10.5194/gmd-9-1937-2016, 2016.

Farquhar, G. D., von Caemmerer, S., and Berry, J. A.: A biochemical model of photosynthetic CO2 assimilation in leaves of C3 species, Planta, 149, 78–90, https://doi.org/10.1007/bf00386231, 1980.

Gallimore, R., Jacob, R., and Kutzbach, J.: Coupled atmosphere-ocean-vegetation simulations for modern and mid-Holocene climates: role of extratropical vegetation cover feedbacks, Clim. Dyn., 25, 755–776, https://doi.org/10.1007/s00382-005-0054-z, 2005.

Gallimore, R. G. and Kutzbach, J. E.: Role of orbitally induced changes in tundra area in the onset of glaciation, Nature, 381, 503–505, 1996.

Harrison, S. P., Jolly, D., Laarif, F., Abe-Ouchi, A., Dong, B., Herterich, K., Hewitt, C., Joussaume, S., Kutzbach, J. E., Mitchell, J., de Noblet, N., and Valdes, P.: Intercomparison of Simulated Global Vegetation Distributions in Response to 6 kyr BP Orbital Forcing, J. Clim., 11, 2721–2742, 1998.

Harrison, S. P., Bartlein, P. J., Brewer, S., Prentice, I. C., Boyd, M., Hessler, I., Holmgren, K., Izumi, K., and Willis, K.: Climate model benchmarking with glacial and mid-Holocene climates, Clim. Dyn., 43, 671–688, https://doi.org/10.1007/s00382-013-1922-6, 2014.

Hewitt, C. D. and Mitchell, J. F. B.: GCM simulations of the climate of 6 kyr BP : Mean changes and interdecadal variability, J. Clim., 9, 3505–3529, 1996.

Hopcroft, P. O., Valdes, P. J., Harper, A. B., and Beerling, D. J.: Multi vegetation model evaluation of the Green Sahara climate regime, Geophys. Res. Lett., 44, 6804–6813, https://doi.org/10.1002/2017GL073740, 2017.

https://doi.org/10.5194/egusphere-2024-4075
Preprint. Discussion started: 22 January 2025

Hourdin, F., Rio, C., Grandpeix, J.-Y., Madeleine, J.-B., Cheruy, F., Rochetin, N., Jam, A., Musat, I., Idelkadi, A., Fairhead, L., Foujols, M.-A., Mellul, L., Traore, A.-K., Dufresne, J.-L., Boucher, O., Lefebvre, M.-P., Millour, E., Vignon, E., Jouhaud, J., Diallo, F. B., Lott, F., Gastineau, G., Caubel, A., Meurdesoif, Y., and Ghattas, J.: LMDZ6A: The Atmospheric Component of the IPSL Climate Model With Improved and Better Tuned Physics, J. Adv. Model. Earth Syst., 12, e2019MS001892, https://doi.org/10.1029/2019MS001892, 2020.

Jolly, D., Prentice, I. C., Bonnefille, R., Ballouche, A., Bengo, M., Brenac, P., Buchet, G., Burney, D., Cazet, J.-P., Cheddadi, R., Edohr, T., Elenga, H., Elmoutaki, S., Guiot, J., Laarif, F., Lamb, H., Lezine, A.-M., Maley, J., Mbenza, M., Peyron, O., Reille, M., Reynaud-Ferrera, I., Riollet, G., Ritchie, J. C., Roche, E., Scott, L., Ssemmanda, I., Straka, H., Umer, M., Van Campo, E., Vilimumbala, S., Vincens, A., and Waller, M.: Biome reconstruction from pollen and plant macrofossil data for Africa and the Arabian peninsula at 0 and 6 ka., J. Biogeogr., 25, 1007–1028, 1998.

Joussaume, S. and Taylor, K. E.: Status of the Paleoclimate Modeling Intercomparison Project, Proc. First Int. AMIP Sci. Conf. WCRP-92 Monterey USA, 425–430, 1995.

Joussaume, S., Taylor, K. E., Braconnot, P., Mitchell, J. F. B., Kutzbach, J. E., Harrison, S. P., Prentice, I. C., Broccoli, A. J., Abe-Ouchi, A., Bartlein, P. J., Bonfils, C., Dong, B., Guiot, J., Herterich, K., Hewitt, C. D., Jolly, D., Kim, J. W., Kislov, A., Kitoh, A., Loutre, M. F., Masson, V., McAvaney, B., McFarlane, N., de Noblet, N., Peltier, W. R., Peterschmitt, J. Y., Pollard, D., Rind, D., Royer, J. F., Schlesinger, M. E., Syktus, J., Thompson, S., Valdes, P., Vettoretti, G., Webb, R. S., and Wyputta, U.: Monsoon changes for 6000 years ago: Results of 18 simulations from the Paleoclimate Modeling Intercomparison Project (PMIP), Geophys. Res. Lett., 26, 859–862, https://doi.org/10.1029/1999gl900126, 1999.

Kageyama, M., Braconnot, P., Harrison, S. P., Haywood, A. M., Jungclaus, J. H., Otto-Bliesner, B. L., Peterschmitt, J. Y., Abe-Ouchi, A., Albani, S., Bartlein, P. J., Brierley, C., Crucifix, M., Dolan, A., Fernandez-Donado, L., Fischer, H., Hopcroft, P. O., Ivanovic, R. F., Lambert, F., Lunt, D. J., Mahowald, N. M., Peltier, W. R., Phipps, S. J., Roche, D. M., Schmidt, G. A., Tarasov, L., Valdes, P. J., Zhang, Q., and Zhou, T.: The PMIP4 contribution to CMIP6 – Part 1: Overview and over-arching analysis plan, Geosci Model Dev, 11, 1033–1057, https://doi.org/10.5194/gmd-11-1033-2018, 2018.

Krinner, G., Viovy, N., de Noblet-Ducoudre, N., Ogee, J., Polcher, J., Friedlingstein, P., Ciais, P., Sitch, S., and Prentice, I. C.: A dynamic global vegetation model for studies of the coupled atmosphere-biosphere system, Glob. Biogeochem. Cycles, 19, 2005.

Levis, S., Bonan, G. B., and Bonfils, C.: Soil feedback drives the mid-Holocene North African monsoon northward in fully coupled CCSM2 simulations with a dynamic vegetation model, Clim. Dyn., 23, 791–802, 2004.

Liu, Z. Y., Zhu, J., Rosenthal, Y., Zhang, X., Otto-Bliesner, B. L., Timmermann, A., Smith, R. S., Lohmann, G., Zheng, W. P., and Timm, O. E.: The Holocene temperature conundrum, Proc. Natl. Acad. Sci. U. S. A., 111, E3501–E3505, https://doi.org/10.1073/pnas.1407229111, 2014.

Madec, Gurvan, Bourdallé-Badie, R., Bouttier, P.-A., Bricaud, C., Bruciaferri, D., Calvert, D., Chanut, J., Clementi, E., Coward, A., Delrosso, D., Ethé, C., Flavoni, S., Graham, T., Harle, J., Iovino, D., Lea, D., Lévy, C., Lovato, T., Martin, N., Masson, S., Mocavero, S., Paul, J., Rousset, C., Storkey, D., Storto, A., and Vancoppenolle, M.: NEMO ocean engine, https://doi.org/10.5281/ZENODO.1472492, 2017.

https://doi.org/10.5194/egusphere-2024-4075
Preprint. Discussion started: 22 January 2025

Manabe, S. and Wetherald, R. T.: The Effects of Doubling the CO_2 Concentration on the climate of a General Circulation Model, J. Atmospheric Sci., 32, 3–15, https://doi.org/10.1175/1520-0469(1975)032<0003:TE-ODTC>2.0.CO;2, 1975.

Marsicek, J., Shuman, B. N., Bartlein, P. J., Shafer, S. L., and Brewer, S.: Reconciling divergent trends and millennial variations in Holocene temperatures, Nature, 554, 92, https://doi.org/10.1038/nature25464 https://www.nature.com/articles/nature25464#supplementary-information, 2018.

Milly, P. C. D.: Potential Evaporation and Soil Moisture in General Circulation Models, J. Clim., 5, 209–226, https://doi.org/10.1175/1520-0442(1992)005<0209:peasmi>2.0.co;2, 1992.

de Noblet, N., Prentice, I. C., Joussaume, S., Texier, D., Botta, A., and Haxeltine, A.: Possible role of atmosphere-biosphere interactions in triggering the last glaciation, Nature, 23, 3191–3194, 1996.

Otto, J., Raddatz, T., and Claussen, M.: Climate variability-induced uncertainty in mid-Holocene atmosphere-ocean-vegetation feedbacks, Geophys. Res. Lett., 36, https://doi.org/L23710 10.1029/2009gl041457, 2009a.

Otto, J., Raddatz, T., Claussen, M., Brovkin, V., and Gayler, V.: Separation of atmosphere-ocean-vegetation feedbacks and synergies for mid-Holocene climate, Glob. Biogeochem. Cycles, 23, https://doi.org/Artn L09701 Doi 10.1029/2009gl037482, 2009b.

Otto, J., Raddatz, T., and Claussen, M.: Strength of forest-albedo feedback in mid-Holocene climate simulations, Clim Past, 7, 1027–1039, https://doi.org/10.5194/cp-7-1027-2011, 2011.

Otto-Bliesner, B., Braconnot, P., Harrison, S., Lunt, D., Abe-Ouchi, A., Albani, S., Bartlein, P., Capron, E., Carlson, A., Dutton, A., Fischer, H., Goelzer, H., Govin, A., Haywood, A., Joos, F., LeGrande, A., Lipscomb, W., Lohmann, G., Mahowald, N., Nehrbass-Ahles, C., Pausata, F., Peterschmitt, J.-Y., Phipps, S., Renssen, H., and Zhang, Q.: The PMIP4 contribution to CMIP6 – Part 2: Two interglacials, scientific objective and experimental design for Holocene and Last Interglacial simulations, Geosci. Model Dev., 10, 3979–4003, https://doi.org/10.5194/gmd-10-3979-2017, 2017.

Pausata, F. S. R., Zhang, Q., Muschitiello, F., Lu, Z., Chafik, L., Niedermeyer, E., Stager, C., Cobb, K., and Liu, Z.: Greening of the Sahara suppressed ENSO activity during the mid-Holocene, Nat. Commun., 8, 1, https://doi.org/citeulike-article-id:14517098, 2017.

Prentice, I. C., Guiot, J., Huntley, B., Jolly, D., and Cheddadi, R.: Reconstructing biomes from palaeoecological data: a general method and its application to European pollen data at 0 and 6 ka, Clim. Dyn., 12, 185–194, 1996.

Rousset, C., Vancoppenolle, M., Madec, G., Fichefet, T., Flavoni, S., Barthélemy, A., Benshila, R., Chanut, J., Levy, C., Masson, S., and Vivier, F.: The Louvain-La-Neuve sea ice model LIM3.6: global and regional capabilities, Geosci. Model Dev., 8, 2991–3005, https://doi.org/10.5194/gmd-8-2991-2015, 2015.

Sellers, P. J., Heiser, M. D., and Hall, F. G.: Relations between surface conductance and spectral vegetation indices at intermediate (100 m^2 to 15 km^2) length scales, J. Geophys. Res. Atmospheres, 97, 19033–19059, https://doi.org/10.1029/92jd01096, 1992.

Sherwood, S. C., Webb, M. J., Annan, J. D., Armour, K. C., Forster, P. M., Hargreaves, J. C., Hegerl, G., Klein, S. A., Marvel, K. D., Rohling, E. J., Watanabe, M., Andrews, T., Braconnot, P., Bretherton, C. S., Foster, G. L., Hausfather, Z., von der Heydt, A. S., Knutti, R., Mauritsen, T., Norris, J. R., Proistosescu, C., Rugenstein, M., Schmidt, G. A., Tokarska, K. B., and Zelinka, M. D.: An Assessment of Earth's Climate Sensitivity Using Multiple Lines of Evidence, Rev. Geophys. Wash. DC 1985, 58, e2019RG000678-e2019RG000678, https://doi.org/10.1029/2019rg000678, 2020.

Sitch, S., Smith, B., Prentice, I. C., Arneth, A., Bondeau, A., Cramer, W., Kaplan, J. O., Levis, S., Lucht, W., Sykes, M. T., Thonicke, K., and Venevsky, S.: Evaluation of ecosystem dynamics, plant geography and terrestrial carbon cycling in the LPJ dynamic global vegetation model, Glob. Change Biol., 9, 161–185, https://doi.org/10.1046/j.1365-2486.2003.00569.x, 2003.

Taylor, K. E., Crucifix, M., Braconnot, P., Hewitt, C. D., Doutriaux, C., Broccoli, A. J., Mitchell, J. F. B., and Webb, M. J.: Estimating shortwave radiative forcing and response in climate models, J. Clim., 20, 2530–2543, https://doi.org/Doi 10.1175/Jcli4143.1, 2007.

Texier, D., de Noblet, N., Harrison, S. P., Haxeltine, A., Jolly, D., Joussaume, S., Laarif, F., Prentice, I. C., and Tarasov, P.: Quantifying the role of biosphere-atmosphere feedbacks in climate change: coupled model simulations for 6000 years BP and comparison with palaeodata for northern Eurasia and northern Africa, Clim. Dyn., 13, 865–882, 1997.

Thompson, A. J., Zhu, J., Poulsen, C. J., Tierney, J. E., and Skinner, C. B.: Northern Hemisphere vegetation change drives a Holocene thermal maximum, Sci. Adv., 8, eabj6535, https://doi.org/10.1126/sciadv.abj6535, 2022.

Vancoppenolle, M., Fichefet, T., and Goosse, H.: Simulating the mass balance and salinity of Arctic and Antarctic sea ice. 2. Importance of sea ice salinity variations, Ocean Model., 27, 54–69, https://doi.org/10.1016/j.ocemod.2008.11.003, 2009.

Wohlfahrt, J., Harrison, S. P., and Braconnot, P.: Synergistic feedbacks between ocean and vegetation on mid- and high-latitude climates during the mid-Holocene, Clim. Dyn., 22, 223–238, https://doi.org/DOI 10.1007/s00382-003-0379-4, 2004.

Yin, X. and Struik, P. C.: C_3 and C_4 photosynthesis models: An overview from the perspective of crop modelling, NJAS Wagening. J. Life Sci., 57, 27–38, https://doi.org/10.1016/j.njas.2009.07.001, 2009.

https://doi.org/10.5194/egusphere-2024-4075
Preprint. Discussion started: 22 January 2025

6 Table

Configuration name	Land surface model configuration	Period	Initial state Ocean + atmosphere	Length
V1 (Vdyn00)	bareold, photoCM6s	H6k	As for the IPSLCM6 PMIP4 simulation*	1000
		PI	Year 1870 of IPSLCM6 PI simulation [+]	1000
V2 (Vdyn17)	barenew, photoCM5	H6k	As for the IPSLCM6 PMIP4 simulation*	600
		PI	Year 1870 of IPSLCM6 PI simulation [+]	400
V3 (Vdyn21)	barenew, photoCM5, *tcrit*	H6k	As for the IPSLCM6 PMIP4 simulation*	600
		PI	Year 1870 of IPSLCM6 PI simulation [+]	700
V4 (Vdyn28)	barenew, photoCM6, *tcrit*	H6k	As for the IPSLCM6 PMIP4 simulation*	1000 years
		PI	Year 300 of V4 H6ka	500 year

Table 1. Characteristics of the different simulations. The different columns refer to the name of the simulation, considering the name in this paper V1 to V4 and our internal simulation number (in parentheses), the initial state and length of the simulation of the mid-Holocene (H6ka) and the preindustrial (PI) simulations. Only the initial state for the ocean-ice-atmosphere component is provide, since all simulations, except V4 PI, start from bare soil. *see Braconnot et al (2021), [+] see Boucher et al. (2020).

Figures

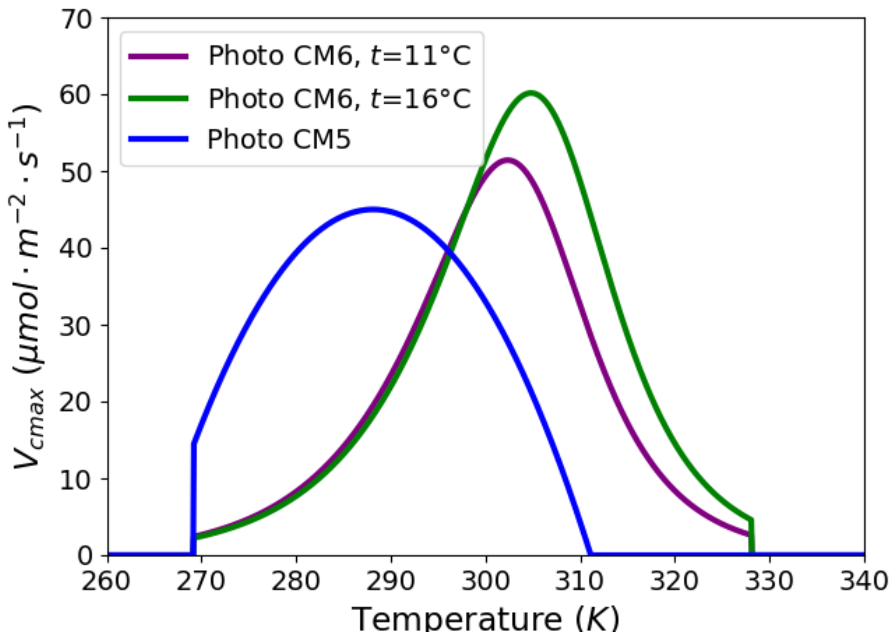

Figure 1: Maximum rate of carboxylation (vcmax, mmol m^{-2} s^{-2}) as a function of surface air temperature (K) for the two photosynthesis parameterization (photoCM5 and photoCM6) and *pft7*.Since phtosynthsis has a dependence on the long term mean monthly temperature, the vcmax curves are plotted toe a mean temperature of 11 and 16°C. Note that with the choice we made, vcmax at 25°C for photoCM6 and the maximum value of photoCM5 are the same. See text for details on the parameterizations.

https://doi.org/10.5194/egusphere-2024-4075
Preprint. Discussion started: 22 January 2025

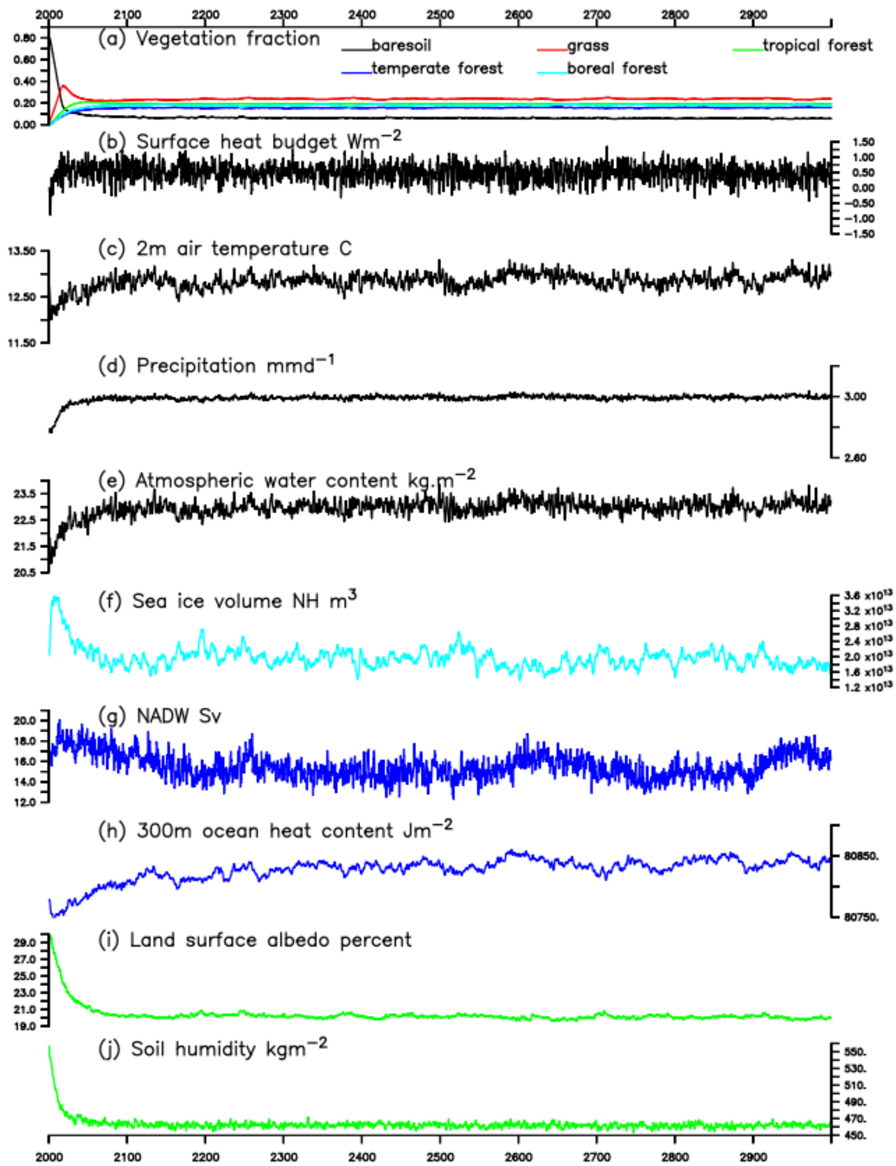

Figure 2. Adjustment time for the V4 mid-Holocene simulation, considering (a) the coverage (fraction) of 4 major vegetation types (grass, tropical forest, temperate forest, and boreal forest) and bare soil, and a subset of climate variables in the atmosphere (black), including (b). surface heat budget (W m^{-2}), (c) 2m air temperature (°C), (d) precipitation (mm d^{-1}), (e) atmospheric water content (kg m^{-2}), in the sea ice (light blue), including (f)in sea ice volume (m^{3}) in the northern hemisphere (NH), in the ocean (blue), including (g) the North Atlantic Deep Water formation (NADW, Sv) and (h) the surface 300 m heat content (J m^{-2}), and in the land surface (green), including (i) the land surface albedo (%) and (j) the soil humidity (kg m^{-3}) (see text for details on the initial state).

https://doi.org/10.5194/egusphere-2024-4075
Preprint. Discussion started: 22 January 2025

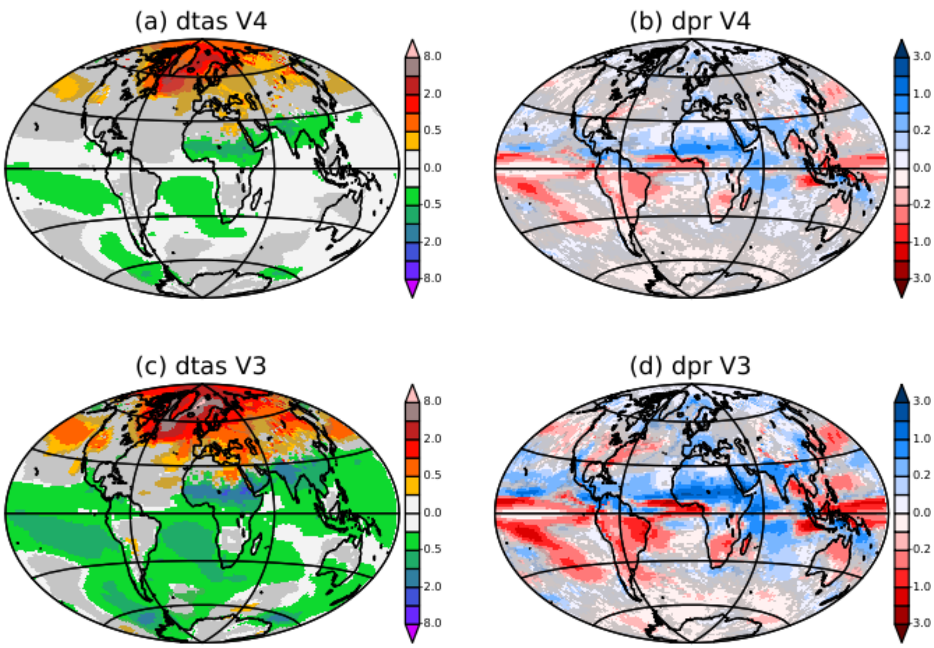

Figure 3. Simulated mid-Holocene (MH) minus Preindustrial (PI) differences for (a) and (c) the 2m air temperature (°C) and (b) and (d) the precipitation (mm d^{-1}) and (a) and (b) the V3 and (c) and (d) V4 model versions. Changes are considered to significant at the 5% level outside the grey zones. The significance is estimated from all combinations of differences between 100-year averages between MH and PI simulations. For these estimates the first 300 years of the simulations are excluded.

https://doi.org/10.5194/egusphere-2024-4075
Preprint. Discussion started: 22 January 2025

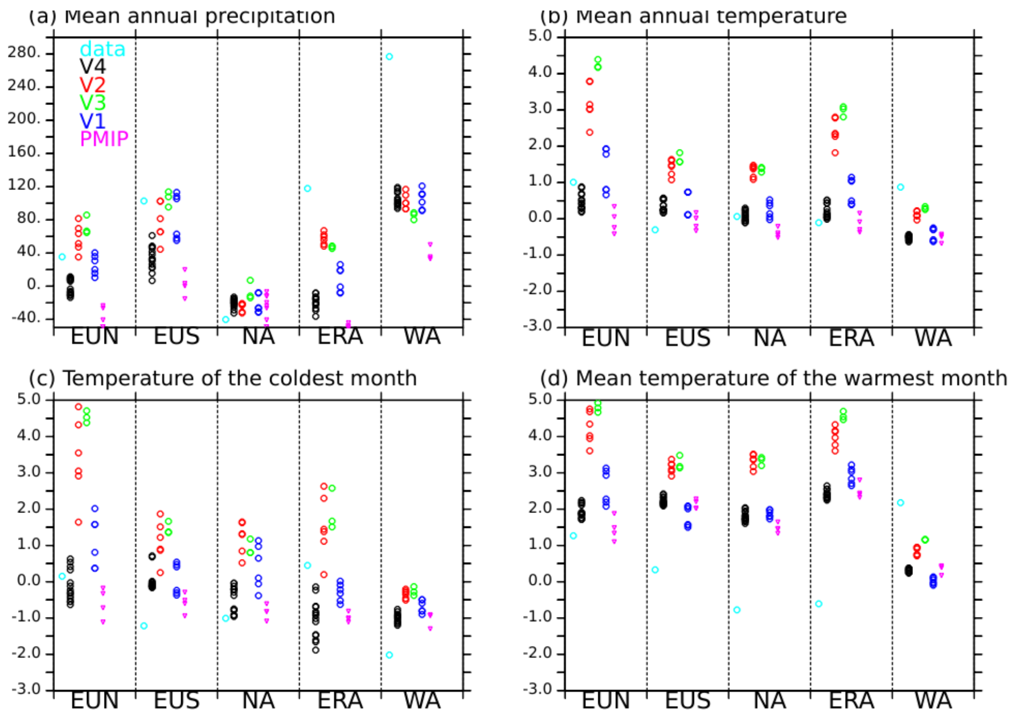

Figure 4. Comparison of the simulated MH minus PI differences with Bartlein et al. (2011) reconstructions for (a) the annual mean precipitation (mm yr^{-1}), (b) the annual mean temperature (°C), (c) the temperature of (c) the coldest month(°C) and (d) the warmest month temperature (C) and 5 selected regions for which the data coverage is high: Northern Europe (EUN), Southern Europe (EUS), North America (NA), Eurasia (ERA) and West Africa (WA).

https://doi.org/10.5194/egusphere-2024-4075
Preprint. Discussion started: 22 January 2025

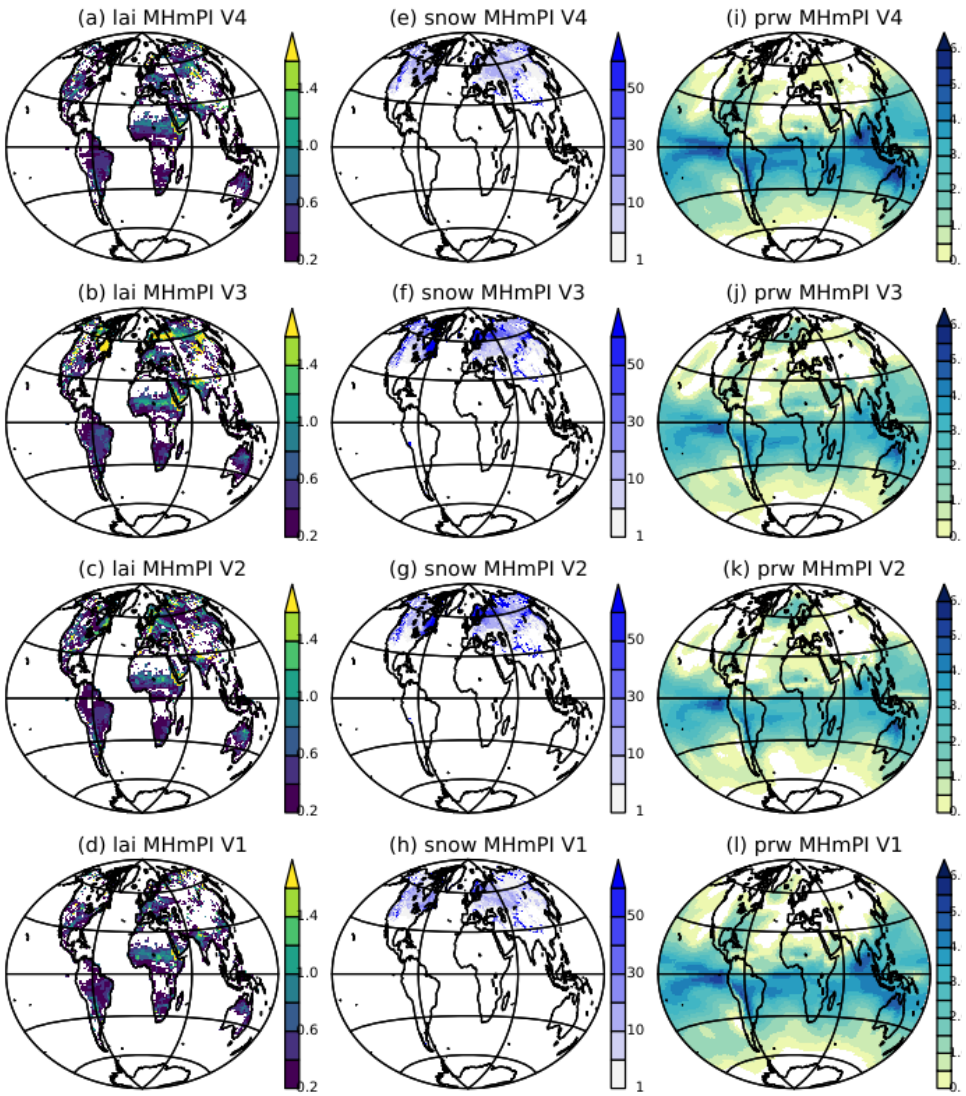

Figure 5: Root mean square difference between Mid Holocene (MH) and Preindustrial climates considering all combinations of 100-year annual mean cycles between the two periods at each grid points for (a) to (d) lai, (d) to (h) the snow mass (kg m^{-2}), and (i) to (l) the atmospheric water content (kg m^{-2}). Not that for snow mass the estimates have been restricted to 100-year monthly differences between February and May, which corresponds to the period where snow feedback over Eurasia is the largest between these two periods.

https://doi.org/10.5194/egusphere-2024-4075
Preprint. Discussion started: 22 January 2025

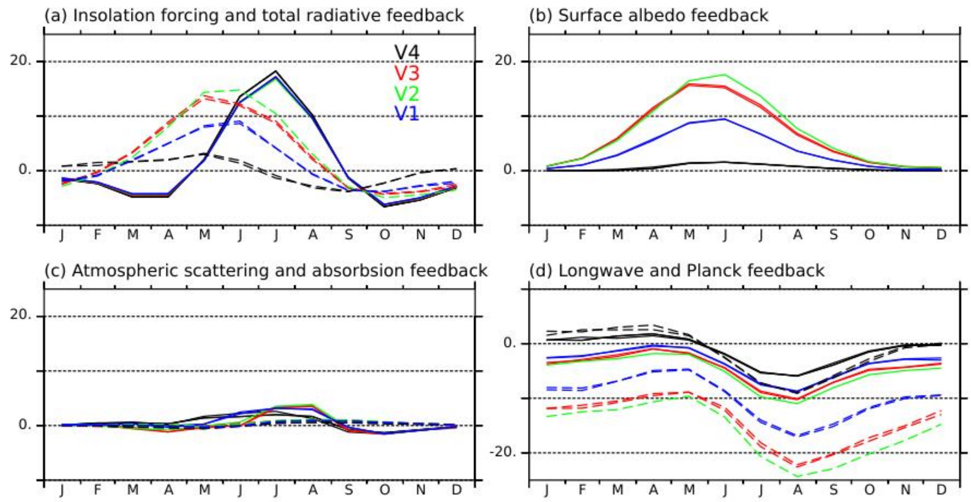

Figure 6: Radiative forcing and feebdacks estimated at Top of the atmosphere (W m^{-2}) between the mid-Holocene and the predindustrial climates over the mid-to high latitudes in the Northern Hemisphere (45°N-80°N) for the four model versions V1 (blue), V2 (green), V3 (red), and V4 (black). (a) Radiative forcing (solid lines) and total radiative feedbacks (dash lines), (b) surface albedo feedback, (c) atmospheric scattering (solid lines) and absorbsion (dash lines) feedbacks, and (d) longwave feedback (solid line) and Plack response (dash lines).

https://doi.org/10.5194/egusphere-2024-4075
Preprint. Discussion started: 22 January 2025

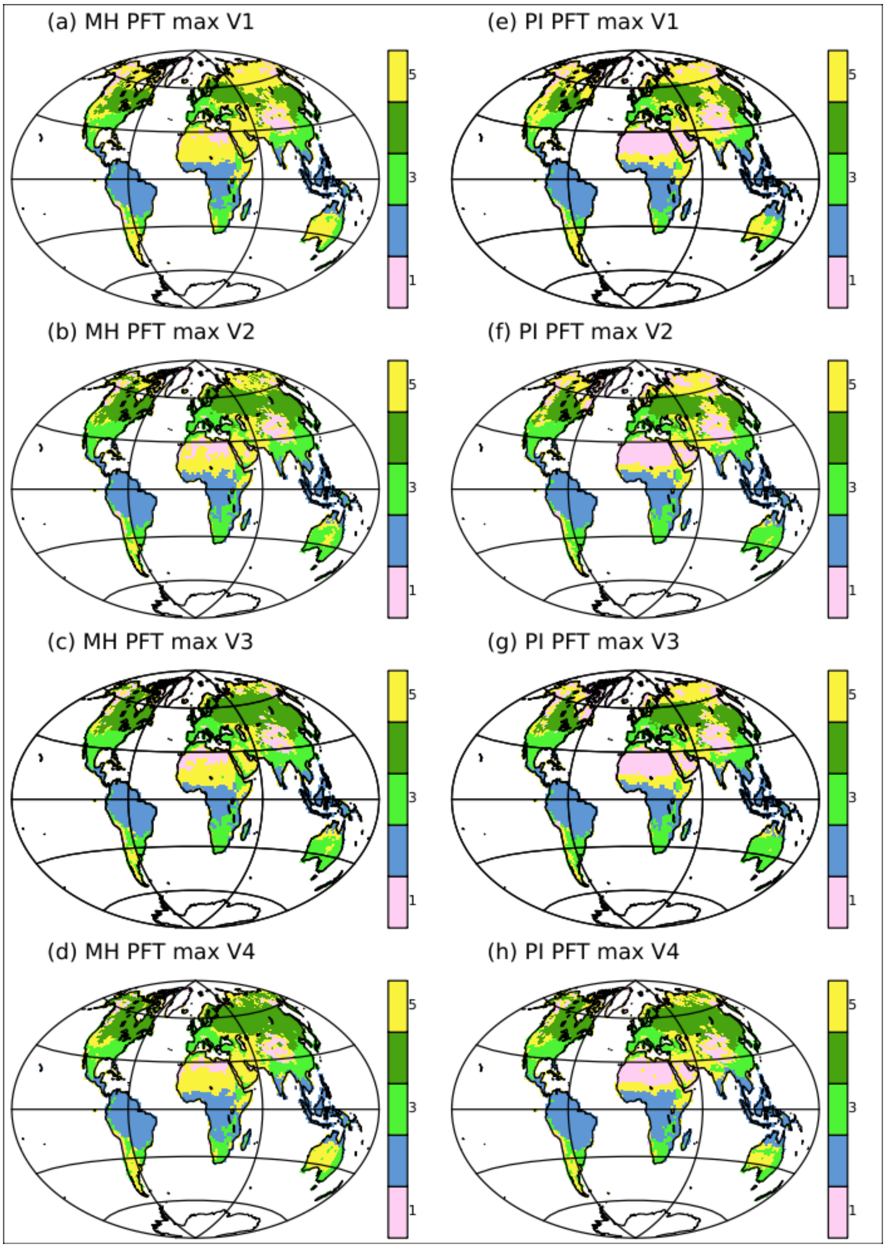

Figure 7. Dominant type of vegetation as simulations by the four model versions for (a) to (d) the mid-Holocene (MH) and ((d) to (f) the preindustrial (PI) climates. For clarity the 15 plant functional types (pft) have been groups into 5 major vegetation types: 1, bare soil; 2. Tropical forest, 3. Temperate forest, 4. Boreal forest, and 5 grass. These maps represent the vegetation average over the length of the simulation, without considering the first 300 year.

https://doi.org/10.5194/egusphere-2024-4075
Preprint. Discussion started: 22 January 2025

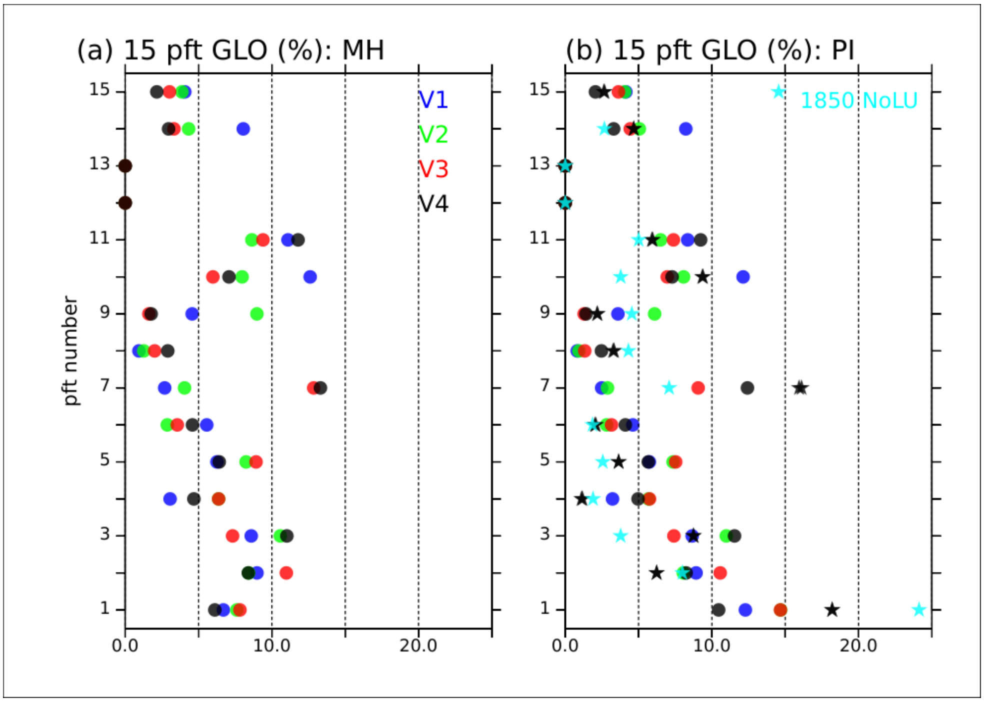

Figure 8. Percentage of global land surface covered by the different types of vegetation (pft) for (a) the mid-Holocene and (b) the preindustrial climates and the four model version (V1: blue, V2: green, V3, red and V4: black). The numbers on the vertical axis refer to the different pft, with 1 for baresoil, 2 for Tropical Broadleaf Evergreen, 3 for Tropical Broadleaf Raingreen, 4 for Temperate Needleleaf Evergreen, 5 for Temperate Broadleaf Evergreen, 6 for Temreferperate Broadleaf Summergreen, 7 for Boreal Needleleaf Evergreen, 8 for Boreal Broadleaf Summergreen, 9 for Boreal Needleleaf Deciduous, 10 for Temperate Natural Grassland (C3), 11 for Natural Grassland (C4), 12 and 13 for crops C3 and crops C4 that are not considered in this study, 14 for Tropical Natural Grassland (C3), and 15 for Boreal Natural Grassland (C3). The stars in (b) represent the pft distribution when only grid points that are not affected by land use in the observed 1850 vegetation map used as reference in simulations with prescribed vegetation, so as to compare the simulated natural vegetation with observations (turqoise for observations, and black for V4).

https://doi.org/10.5194/egusphere-2024-4075
Preprint. Discussion started: 22 January 2025

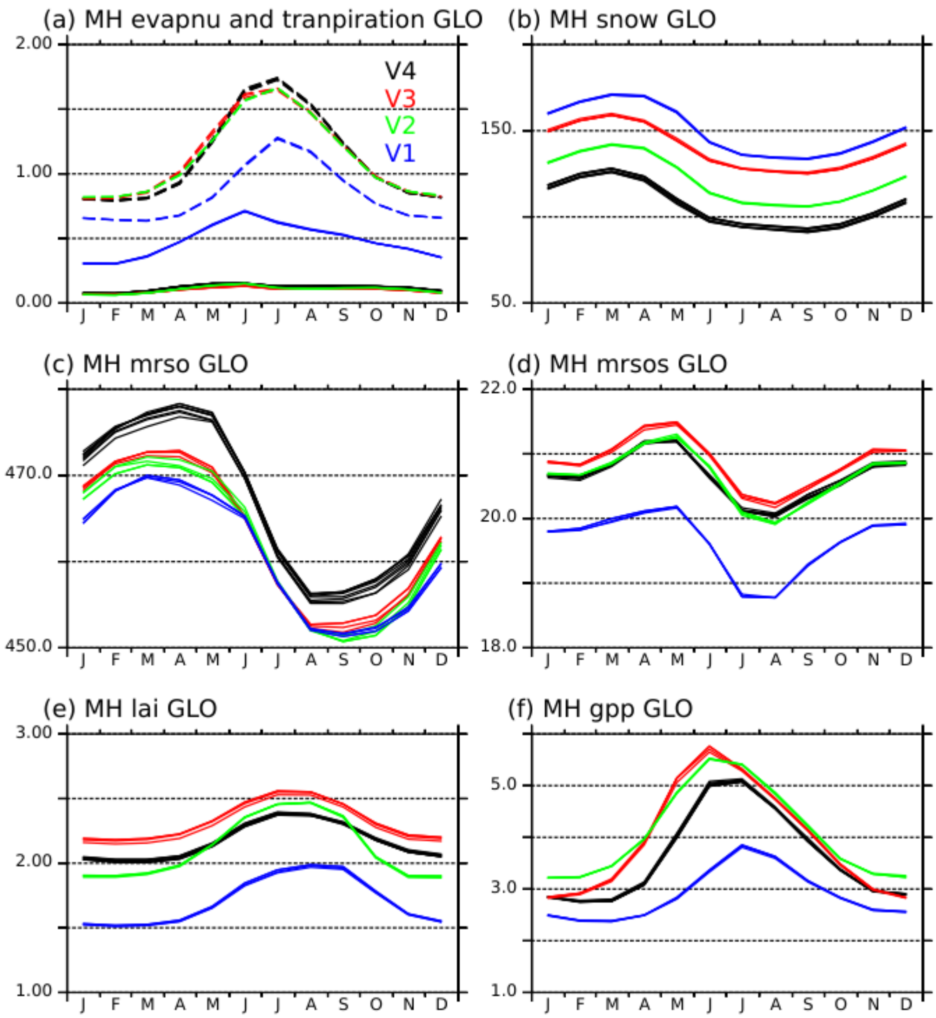

Figure 9. Annual cycle of mid-Holocene (a) bare soil evaporation (mm d^{-1}, solid lines) and transpiration (mm d^{-1}, dash lines), (b) snow mass (kg m^{-2}), (c) total soil moisture (kg m^{-2}), (d) surface soil moisture (kg m^{-2}), (e) leaf area index (lai) and (f) net assimilation of carbon by the vegetation (gpp, gC m^{-2} s^{-1}) globally averaged over land for the 4 simulations (V1: blue, V2 : green, V3: red, and V4 : black). All 100 years annual mean cycles, excluding the 300 first years, are plotted for each simulation in order to provide and idea of 100-year variability and show that the differences between the simulations are robust.

https://doi.org/10.5194/egusphere-2024-4075
Preprint. Discussion started: 22 January 2025

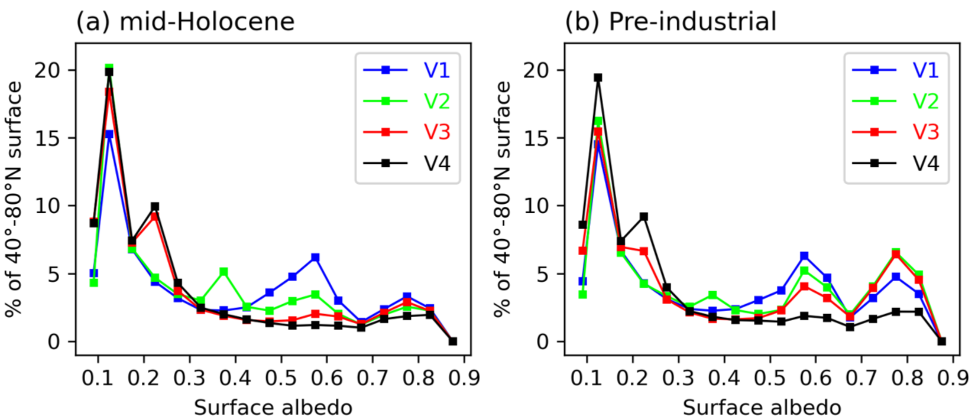

Figure 10: Distribution of the surface albedo (fraction of reflected radiation) simulations with the different version of the IPSL model, considering all grid points between 45°N and 80°N and months, for (a) the mid-Holocene and (b) the preindustrial climates. For each albedo bin, the value represents the percentage of surface with this particular albedo value. The first bin (lower value) corresponds to the ocean portion in the considered grid box where ice or land is also present. The higher values correspond to sea ice whereas values between 0.1 and 0.3 correspond to vegetation and bare soil, and values between 0.3 and 0.7 to different mixtures of vegetation and snow albedo. The surface albedo has been estimated using the surface upward and downward solar radiation.

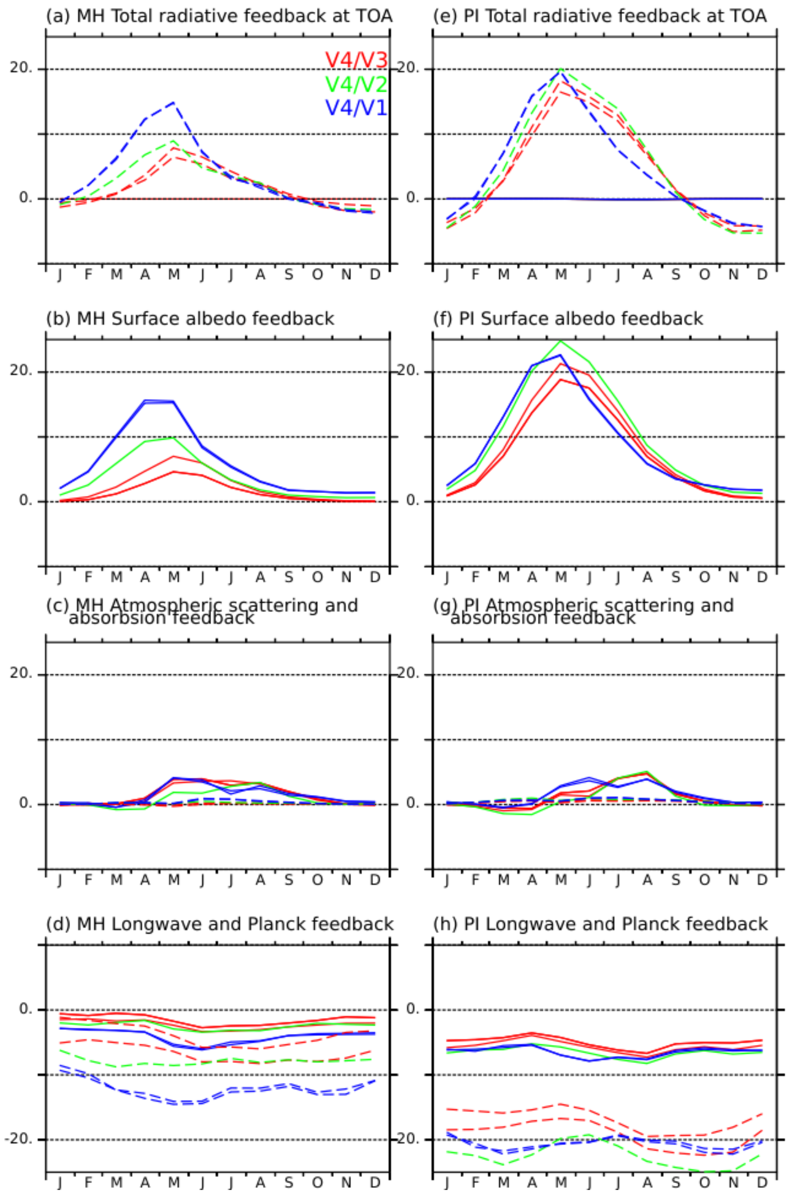

Figure 11. Estimation of radiative feedbacks (W m^{-2}) induced by the differences in the land surface model and vegetation between the V1 (blue), the V2 (green), the V3 (red) and the V4 model versions used as reference, for (a) to (d) the mid-Holocene simulations (MH) and (e) to ((h) the preindustrial simulations. Positive (negative) value indicate that more energy is entering (leaving) the climate system in V4 compared to the other version at the top of the atmosphere. As in figure 7 the different panels consider (a) and (e) the total radiative feedbacks, (b) and (f) the surface albedo feedback, (c) and (g) the atmospheric scattering (solid lines) and absorption (dash lines), and (d) and (h) the outgoing longwave radiation feedback (solid lines) and the Planck response (dash lines).

https://doi.org/10.5194/egusphere-2024-4075
Preprint. Discussion started: 22 January 2025

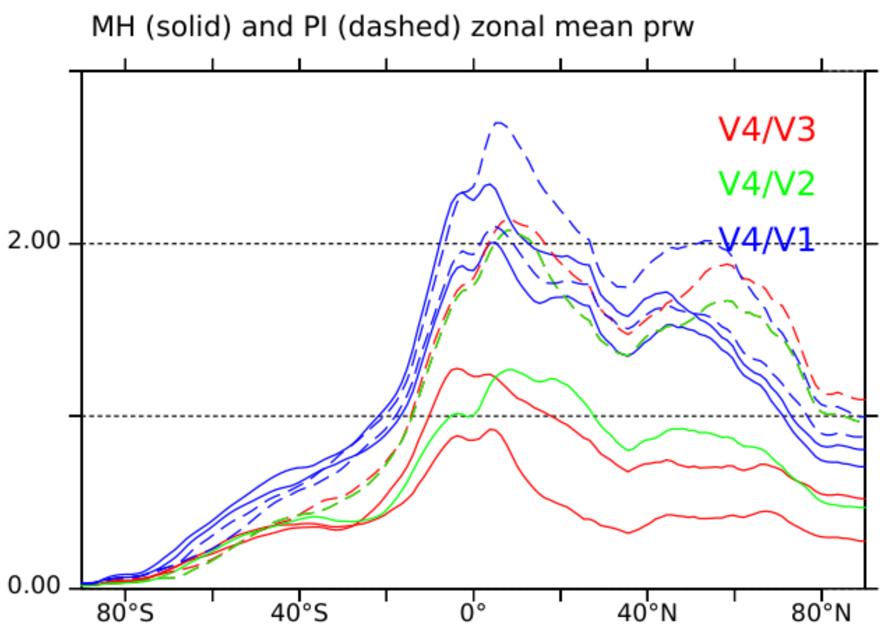

Figure 12: Difference between the zonal average of the integrated atmospheric water content (kg m^{-2}) as simulated using the V4 version of the model and the V1 version (blue), the V2 version (green) and the V3 version (red). The solid lines stand for the differences computed for the mid-Holocene climate and the dotted lines for the preindustrial climate. The different lines for a given estimate represent uncertainties computed using estimates from two different 100-year averages between simulations.

https://doi.org/10.5194/egusphere-2024-4075
Preprint. Discussion started: 22 January 2025

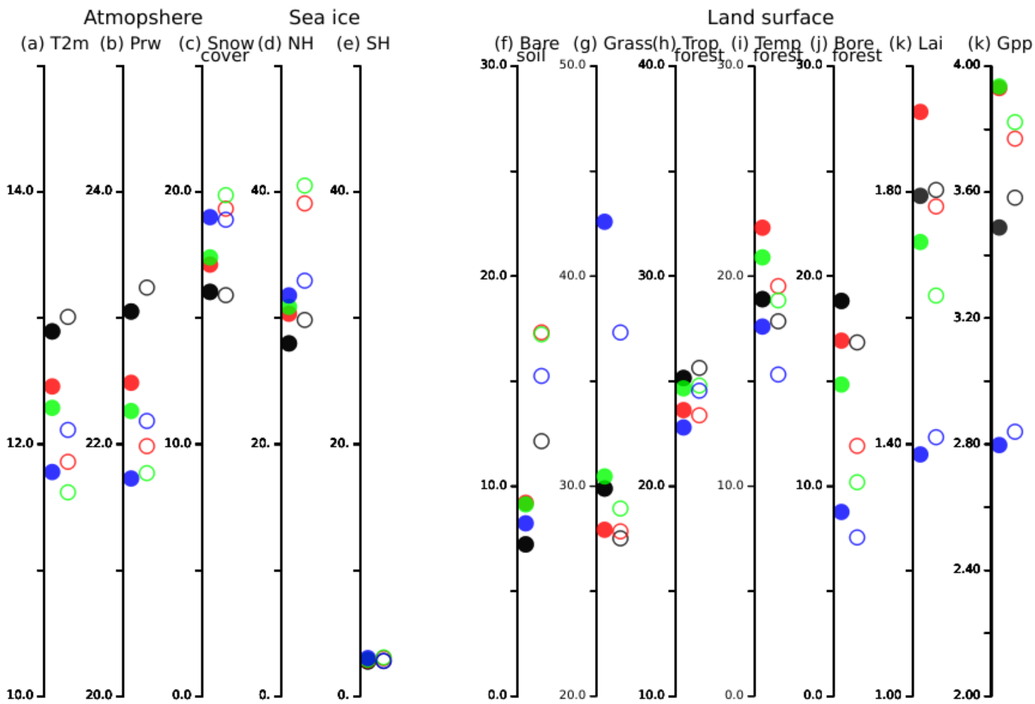

1013

1014 Figure 13. Mid-Holocene (full circles) and Preindustrial (circle) global annual mean for (a) surface air temperature
1015 (T2m, °C), (b) Precipitable water content (kg m^{-2}), (c) snow cover over land (%), (d) bare soil (%), (e) grass (%),
1016 (f) tropical forest (%), (g) temperate forest (%), (h) boreal forest (%), (i) lai, and (j) gross primary production
1017 (10^5 gC m^{-2} $s^{-1)}$ and the four model versions (V1 : blue, V2: green, V3 : red and V4 : black).

1018

1019

1020

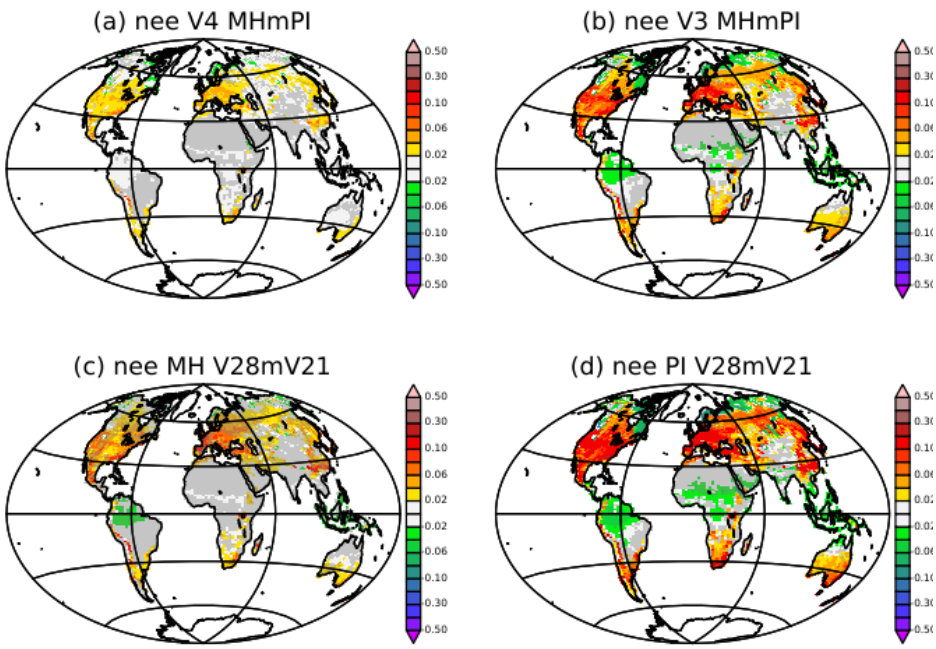

Figure 14. Net carbon flux from the vegetation (kg m^{-2} s) difference between (a) the mid-Holocene and the preindustrial climates as simulated with version V4, (b) the mid-Holocene and the preindustrial climate as simulated by with version V3, (c) the version V4 and V3 of the mid-Holocene simulations, and (d) the version V4 and V3 of the preindustrial climate. Changes are considered to be significant at the 5% level outside the grey zones. The significance is estimated from all combinations of differences between 100-year averages between the simulations considered in each panel. For these estimates the first 300 years of the simulations are excluded.